Table 1. Synthesis of **4a–d** with different contents of gadolinium chelates

	Introduction ratio of DOTA[a] (mol%)	Mn[b] ($\times 10^5$)	M_w/M_n[b]	Gd[c] (wt%)	Gd/DOTA (mol%)	FITC label	R_1 (mM^{-1} s^{-1})
4a	13.2	1.6	1.1	12.0	70.0	–	7.1
4b	7.5	1.1	1.2	9.2	69.1	–	6.2
4c	3.6	1.2	1.2	5.8	67.0	–	6.2
4d	12.9	—	—	9.3	53.9	+	7.0

[a]Scheme 1, $m/n \times 100$.
[b]Determined by size exclusion chromatography using 0.25 mM phosphate buffer as eluent with polystyrene standards.
[c]Determined by inductively coupled plasma atomic emission spectroscopy measurement.

2.3. Cytotoxicity of Gd–PVA to NIH-3T3 cells and cell labeling by electroporation

Gd–PVA **4b** was used for a cytotoxicity assay since FITC introduced to **4d** obstructs the accurate WST-1 assay. The viability of NIH-3T3 cells in the presence of **4b** was not affected even at high concentrations (10 mM; polymer unit concentration in culture medium) for up to 3 days (see Supplementary Information). The low affinity of PVA (24) might suppress the interaction of Gd–PVA with the cell membrane and decrease the cytotoxicity. In fact, weak interaction was demonstrated by a simple experiment as follows. Compound **4d** was added to the culture medium of NIH-3T3 cells, and the cells were incubated for 1 h. After washing with PBS three times, no fluorescence induced by **4d** was observed, indicating that **4d** was unable to attach to the cell membrane or enter the cells spontaneously.

To deliver such a bio-inert substance into cells, we selected an electroporation method that is mainly used to transfect DNA into cells. Since this method can introduce a large amount of polymeric substances into any kind of cells nonspecifically with low cytotoxicity, it is suitable for labeling various cells including established cell lines, somatic stem cells, or even embryonic stem cells for cell transplantation (25,26). When electroporation was carried out, the concentration of Gd–PVA in culture medium was set to 10 mM (polymer unit concentration) based on the result of the cytotoxicity assay.

Figure 2 shows bright field and fluorescent photomicrographs of NIH-3T3 cells 3 days after electroporation with **4d**. Almost all cells were labeled efficiently, and the intracellular **4d** was interestingly located only in the cytosolic compartment of NIH-3T3 cells even after cell proliferation. This intracellular distribution pattern is different from that for endocytosis, which is made from bright dots.

The stability of Gd–PVA in NIH-3T3 cells was assessed by measuring the total fluorescence intensity of the growing NIH-3T3 cells with time. The number of Gd(III) molecules in one cell calculated from the fluorescence intensity was 7.3×10^8 per cell just after electroporation. Cells were cultured for a given period of time without subculture and then lysed. Before the cells were lysed, they were washed by PBS sufficiently to eliminate any **4d** leaching from them. Figure 3 represents the total fluorescence intensity of **4d** in NIH-3T3 cells (solid circle) and cellular proliferation rates (open circle). Fluorescence derived from **4d** in cells showed no significant change over 10 days, and the labeled cells grew well. These results show that **4d** can remain in the cytosolic compartment stably for a long period of time without having any effect on cell proliferation.

2.4. *In vitro* T_1-weighted MR measurements of the labeled NIH-3T3

Figure 4a shows an MR image of the NIH-3T3 cell suspensions at 4.7 T. Compound **4d**-labeled NIH-3T3 cell suspension, non-labeled NIH-3T3 cell suspension and cell-free and Gd-free medium were left at rest for 1 day to allow the cells to be precipitated to the bottom of the test tube. Clear signal enhancement in tube 1 at slice B passing through the precipitated cells was seen. On the other hand, no signal was observed in tube 1 at slice A, which indicates that **4d** did not leak out of the cells and that **4d** in cells gives sufficient MR contrast irrespective of the small amount of free water in the cells

To examine the cell density dependence of signal enhancement, we next acquired MR images of **4d**-labeled NIH-3T3 cells at different densities in agarose gel, which was used to fix the transplanted cells in the experiment involving the injection of cells into a rat (Fig. 4b). MRI can depict at least 3.5×10^6 NIH-3T3

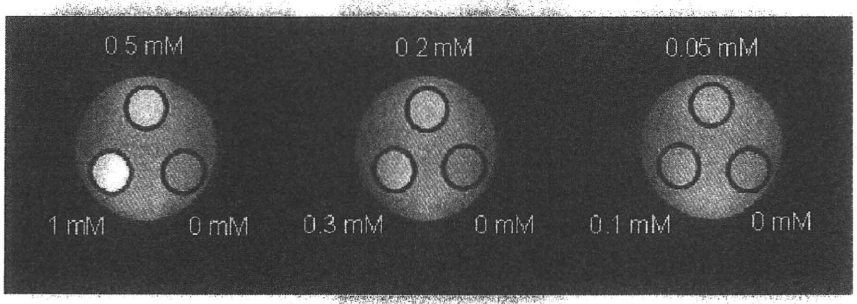

Figure 1. *In vitro* T_1-weighted MR measurements of **4d** in water at 4.7 T at the concentrations of 0, 0,05, 0.1, 0.2, 0.3, 0.5, and 1.0 mM. Three test tubes containing different concentrations were fixed vertically. A horizontal section was scanned. These images were acquired using a 2 D spin echo sequence with a TR of 2000 ms and a TE of 16 ms. These images were displayed using the same window level and window width.

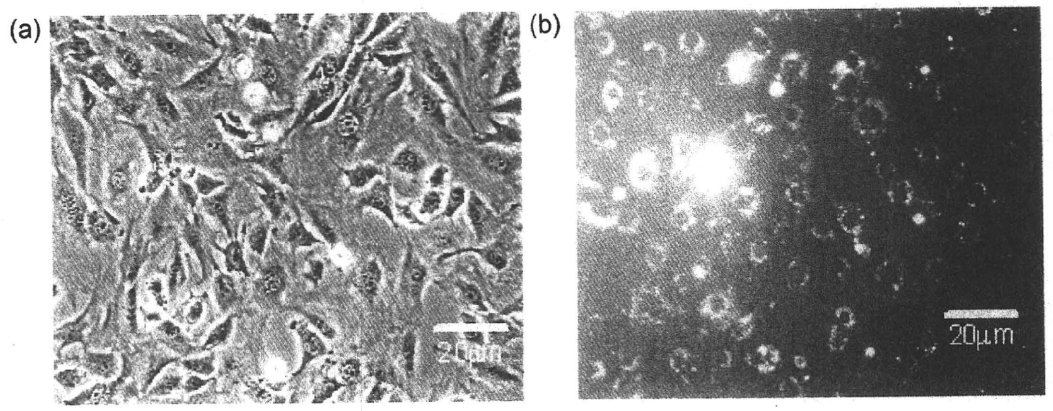

Figure 2. (a) Phase image and (b) fluorescent image of NIH-3T3 cells labeled with **4d** (FITC-Gd-PVA) at 3 days after electroporation. After electroporation, cells were washed three times by PBS. The bright ring forms showed cytosolic compartments in the fluorescent image. The scale bar represents 20 μm.

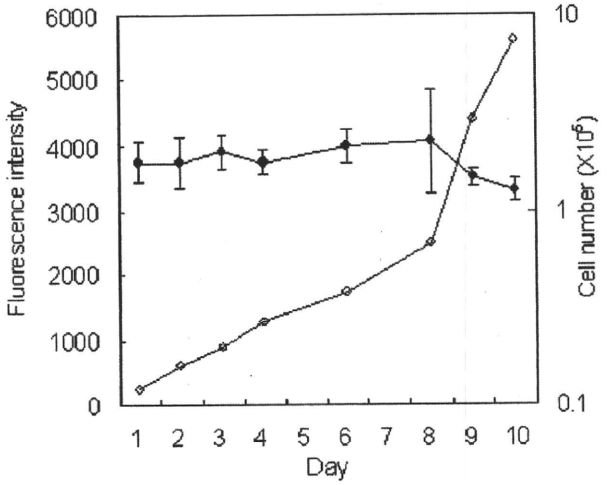

Figure 3. Changes in fluorescence intensity of **4d** existing in total NIH-3T3 cells in culture (solid circle) and the number of cells (open circle) measured over the course of the 10 days following electroporation. Fluorescence intensity is proportional to the amount of **4d** in total cells.

cells. The number of cells transplanted to the rat ischemic hind limb model (27) or infarcted myocardium swine model (28) was 1×10^7 or 5×10^7, respectively. The sensitivity shown in Fig. 4 revealed that our imaging agent would surely be useful for tracking this range of transplanted cells *in vivo*. Future studies should focus on high labeling efficiency at higher concentrations of **4d** using electroporation or another method.

2.5. *In vivo* fate of free SPIO and free Gd–PVA

To detect the living cells, contrast agents present outside of the labeled cells (free contrast agent) after cell death should be eliminated from the transplantation site. Solutions of **4d** and SPIO injected into the tissue were used as the model for free contrast agents. Solutions of **4d** and SPIO were directly injected into rat femoral muscles, and on days 0, 3 and 6, the MR image was analyzed (Fig. 5). Representative slices are shown in Fig. 5. The bright signal attributed to **4d** weakened rapidly and was observed only slightly on day 3. In contrast, the dark signal due to SPIO remained in the same area and was clearly observed even 10 days after the injection. The same tendency was observed in the other slices. SPIO-derived contrast several days after injection may be attributed to the phagocytes engulfing the injected SPIO, as has been previously reported (22,23). Furthermore, the time courses of the contrast-to-noise ratio (CNR) and the volume of the contrast-enhanced region were evaluated (Fig. 6). For SPIO, the CNR and the volume of the contrast-enhanced region showed no significant decrease over the course of 13 days. In contrast, these same parameters decreased rapidly when **4d** was used. Signal enhancement was observed in only one out of three rats at 4 days after injection. Therefore, the data of **4d** at 4 days have no error bar. Signal

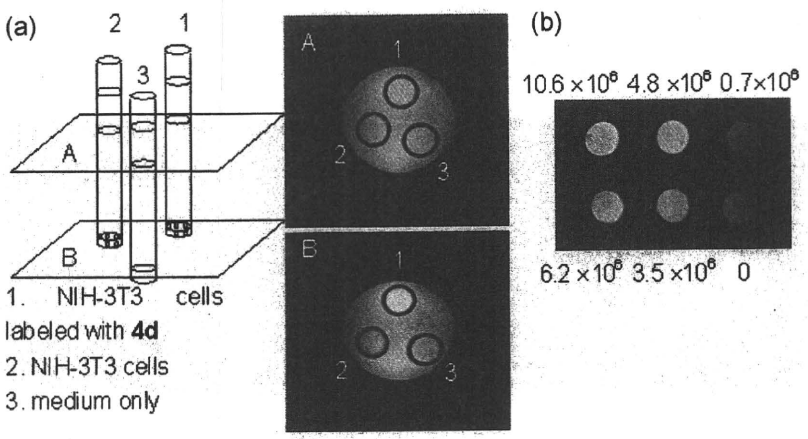

Figure 4. (a) *In vitro* T_1-weighted MR measurements of **4d**-labeled NIH-3T3 cells (tube 1), unlabeled NIH-3T3 (tube 2), and medium (tube 3) at 4.7 T. (b) *In vitro* T_1-weighted image of different numbers of cells labeled with **4d** suspended in 100 μl agarose gel.

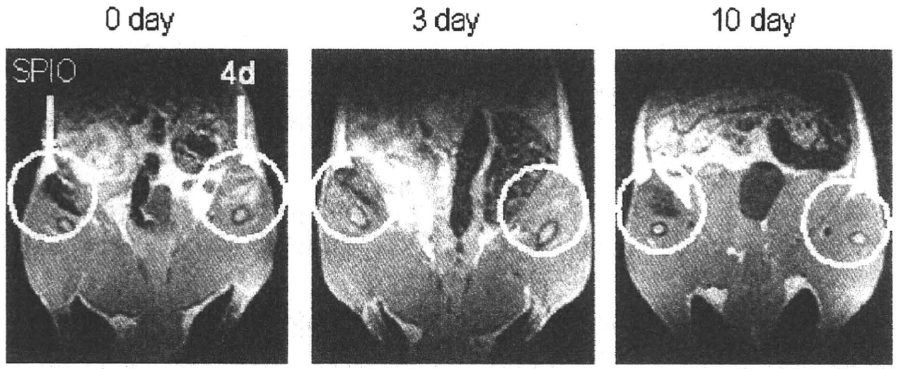

Figure 5. *In vivo* MR measurements after the injection of **4d** solution and SPIO solution into rat femoral muscle at 1.5 T. These images showed the slices passing though the injection site. These images were obtained with a TR of 1500 ms and a TE of 9 ms (FOV, 4 × 8 cm; matrix, 128 × 256; slice thickness, 1 mm; slice gap, 0 mm; number of slices, 35).

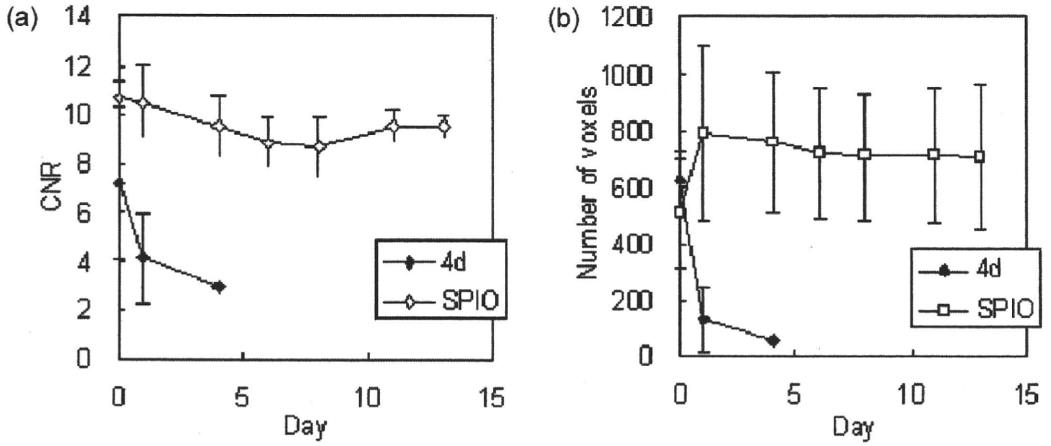

Figure 6. The time course of (a) the contrast-to-noise ratio (CNR) and (b) the number of voxels in the region where bright or dark signals due to contrast agents were observed. Contrast enhancement due to **4d** and SPIO was assessed using T_1- (TE 9 ms, TR 500 ms) and T_2- (TE 20 ms, TR 3 s) weighted images, respectively. The other scanning parameters were the same as in Figure 5. Three rats were examined and treated in the same manner as in Figure 5. CNR was calculated as $(\pi/2)^{1/2}|S_1\text{-}S_2|/S_{air}$, where S_1, S_2 and S_{air} were the mean intensities in the contrast-enhanced region, muscle and air, respectively.

enhancement due to **4d** disappeared completely in all rats at 6 days after injection. These data showed the rapid clearance of Gd–PVA from muscle and the long-term retention of SPIO in muscle. Yamaoka *et al.* reported that the half-life period of radio-labeled PVA (molecular weight of 74 800) after i.m. injection was about 10 h (38). As shown in Fig. 6, the half-life period of free Gd–PVA from the tissue was about 10 hs, which was almost the same as that of PVA. This result suggested that free Gd–PVA behaved like free PVA without interacting with macrophages *in vivo*. It can then be considered that the MR contrast of Gd–PVA is attributable to the living cells *in vivo*.

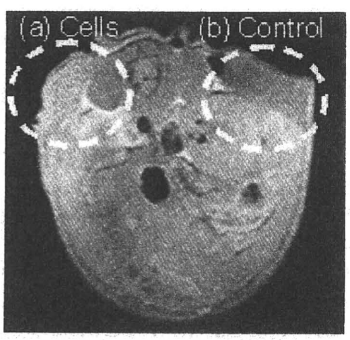

Figure 7. Preliminary *in vivo* T_1-weighted MR measurements of **4d**-labeled NIH-3T3 cells implanted in mice subcutaneously at 2 T. These cells were fixed in agarose gel. (a) 2×10^7 of **4d**-labeled cells suspended in 200 μl agarose gel (b) 200 μl agarose gel only. T_1-weighted images were acquired using a 2D spin echo sequence with a TR of 2000 ms and a TE of 9 ms (FOV, 3 × 6 cm; matrix, 128 × 256; slice thickness, 1 mm) at room temperature.

2.6. Preliminary *in vivo* MR imaging of transplanted NIH-3T3 cells

Figure 7 shows an MR image of a rat that received subcutaneous transplantation of 2×10^7 **4d**-labeled NIH-3T3 cells entrapped in agarose gel and cell-free gel (control) at each side of the back. In this preliminary MR imaging, we used undegradable agarose gel to evaluate the MRI contrast at a known density of cells. Strong contrast enhancement was observed at the area where labeled NIH-3T3 cells were transplanted, while the control gel revealed a dark shadow. These results indicate that transplanted cells can be detected *in vivo* at a cell density of 10^7 cells per 0.1 ml.

3. DISCUSSION

Our goal was to track only the living cells *in vivo* for a long period of time. To this end, an MRI contrast agent with adequate

characteristics for cell labeling and delivery system into the cells is a key factor. Cell labeling using SPIO as a contrast agent was reported in detail by Engberink *et al.* in 2007 (29). They cocultured human monocytes with SPIO suspension at a concentration of 1.0 mg Fe ml^{-1} for 0–6 h. Incubation with SPIO resulted in effective cell labeling by endocytosis, nonspecifically. The detection limit was 0.5×10^6 labeled cells per 250 μl on a 4.7 T MRI scanner. SPIO permits the detection of a small number of cells because of its high sensitivity. In general, however, endocytosed substrates would be exocytosed over time. The MR contrast obtained after SPIO-labeled cell transplantation was not attributed to the transplanted cells but to the macrophages that engulfed the free SPIO (22,23). In this study, MR imaging data for SPIO solution in femoral muscle showed that, even at 10 days after injection, SPIO still remained. These data suggested that SPIO is less suitable for long-term cell tracking. To track the transplanted cells for a long period of time, the labeling agent released upon cell death should be eliminated from the tissue.

Since we found that low-molecular-weight Gd-chelates cannot remain in cells stably (data not shown), water-soluble conjugates of Gd-chelates and a bio inert water-soluble carrier were designed. The characteristics of Gd-containing conjugates including the body distribution pattern are affected by the nature of the carrier polymer. The water-soluble contrast agent is expected to be eliminated from the body once it exits the cells if a truly bio-inert carrier molecule is selected. To track only the living cells, the contrast agents should be designed to be different from the conventional water-soluble imaging agent for vascular inflammation imaging or vascular imaging (30–36).

We selected PVA in this experiment as the carrier material for long-term living cell tracking. Selecting nondegradable PVA as the carrier enabled us to evaluate the potential of the contrast agent in intracellular distribution or in cell tracking for a long period of time. The body distribution of various polymeric carriers has been extensively studied (37,38). Among these carriers, PVA has various advantages as a candidate for use in the biomedical and pharmaceutical fields. Some of these advantages include its characteristics of water solubility, nontoxicity and noncarcinogenicity. The half-life of Gd–PVA was longer than those of other polymers such as dextran, pullulan and gelatin because of an insignificant interaction with macrophages and blood cells (24). This weak interaction with various cells is believed to be responsible for the high hydrophilicity of PVA. Since we proposed novel contrast agents in the present study that would not exit the cells for long-term cell tracking, this weak interaction with the cell membrane was considered to be an advantage.

In the present study, we chose electroporation as a method for delivering Gd–PVA into cells in order to establish a method that is applicable to a variety of cells such as stem cells and primary cells. The material delivery efficiency into cells via nonspecific endocytosis or receptor-mediated encodytosis is probably affected by the cell type. Interestingly, Gd–PVA delivered into cells was localized only in the cytosolic compartment even after cell proliferation (Fig. 2), although the reason for this remains unclear.

One possible issue in living cell tracking, although unlikely to occur, is the uptake of dying cells labeled with **4d** by tissue macrophages that remain in the tissue. To study this possibility, it is necessary to perform an experiment using cells in different states (viable, dying and dead). However, it is difficult to control the states of transplanted cells. We are considering evaluating the effect of macrophages on the fate of Gd–PVA by transplanting irradiated cells with sublethal doses or by xenografting Gd–PVA-labeled cells.

Long-term cell tracking will be feasible due to the high stability of Gd–PVA in cells for a long period of time (Fig. 3). In contrast to SPIO, the free Gd–PVA will be eliminated from the tissue (Fig. 5) when the transplanted cells burst upon cell death. The imaging of only the living cells might be achieved using Gd–PVA.

4. CONCLUSION

The novel MRI contrast agents composed of PVA and Gd showed high relaxivity and low cytotoxicity. The growing rate of NIH-3T3 cells was not affected by the intracellularly delivered Gd–PVA. Furthermore, Gd–PVA was retained stably in cells for at least 10 days. The *in vitro* T_1-weighted MR measurements using NIH-3T3 cells revealed that cells could be visualized under MRI. This *in vivo* study demonstrates for the first time that Gd–PVA has high applicability as a novel contrast agent for tracking only living cells.

5. MATERIALS AND METHODS

5.1. Materials

PVA (M_w: 74,800, degree of saponification 98%) was a kind gift from Kuraray Co. Ltd (Okayama, Japan). 1,4,7,10-Tetraazacyclododecane-1,4,7,10-tetraacetic acid mono(*N*-hydroxysuccinimidyl ester) (DOTA-NHS-ester) was purchased from Macrocyclics (Dallas, TX, USA). FITC-NHS-ester was purchased from Invitrogen (Eugene, OR, USA). Gadolinium chloride ($GdCl_3$) was purchased from Wako Pure Chemical Industries (Osaka, Japan). Resovist was purchased from Nihon Schering (Osaka, Japan). Other reagents and solvents were commercially available and used as received.

5.2. Synthesis of Gd–PVA

The synthetic route and structure of polymeric contrast agents with different introduction ratios of Gd are shown in Scheme 1. A mixture of PVA (**1**; 0.44 g, 10 mmol in monomer unit concentration) and carbonyl diimidazole (5, 7.5, and 10 mmol) was stirred in 80 ml of anhydrous dimethylsulfoxide (DMSO) at room temperature under a nitrogen atmosphere for 4 h. Then, 1,3-propanediamine (50, 75, and 100 mmol) was added to the mixture, further stirred at room temperature for 1 day, and dialyzed with Spectra/Pore membrane (cut-off molecular weight = 1×10^4; Spectrum Laboratories Inc., Rancho Dominguez, CA, USA) in distilled water three times. The remaining solution was lyophilized to give **2**.

^{1}H NMR (D_2O): $\delta = 4.92$ (br, CH_2CHO), 3.92 (br, CH_2CHOH), 3.10 [br, $C(=O)NHCH_2$], 2.79 (br, CH_2NH_2), 1.57 (br, $CHCH_2$, br, $CH_2CH_2CH_2$). The introduction ratios were calculated as the ratio of the integrals of the peaks at 2.79 and 1.57 ppm.

PVA-diamine was reacted with DOTA-NHS-ester (NH_2 of FITC-PVA-diamine: DOTA-NHS-ester = 1:1.5) in 80 ml of anhydrous DMSO at room temperature for 1 day under a nitrogen atmosphere. The reaction mixture was dialyzed in distilled water three times, and lyophilized to give PVA-diamine-DOTA (**3**).

^{1}H NMR (D_2O): $\delta = 5.07$ (br, CH_2CHO), 4.06 (br, CH_2CHOH), 3.86 [br, $C(=O)CH_2N$)] 3.51 [br, $NCH_2C(=O)OH$], 3.24 [br, $C(=O)NHCH_2$, br, CH_2CH_2N], 1.69 (br, $CHCH_2$, br, $CH_2CH_2CH_2$).

The solution of **3** was then treated with the dropwise addition of 1.5 mole equiv. of gadolinium chloride to the DOTA while stirring. The pH was maintained between 6.6 and 7.0 with 1 M NaOH solution and stirred for an additional 24 h at room temperature. The reaction mixture was dialyzed in distilled water three times and lyophilized to give Gd–PVA (**4a–d**).

For labeling Gd–PVA with FITC, PVA–diamine was mixed with a small amount of FITC–NHS–ester (NH_2 of **2**: FITC–NHS–ester = 1: 8×10^{-5}) and stirred in 80 ml of anhydrous DMSO at room temperature for 1 day under a nitrogen atmosphere. The reaction mixture was dialyzed, lyophilized to give FITC-PVA-diamine and subjected to the DOTA reaction as shown in Scheme 1.

5.3. Measurements

^{1}H-NMR spectra were recorded on a 300 MHz NMR spectrometer (Gemini2000/300; Varian Inc., CA, USA) with a sample concentration of 8 mg per 800 μl. Size exclusion chromatography analysis was carried out using Shimadzu Gel Permeation Chromatography System apparatus equipped with a refractive index and UV detectors under the following conditions: TSKgel G6000PWXL and G3000PWXL columns and 0.067 M PBS eluent at a flow rate of 0.3 ml min^{-1} at 40°C (Tosoh, Tokyo, Japan) with a sample concentration of 1 mg per 100 μl. The concentration of the paramagnetic species [Gd(III)] was measured by inductively coupled plasma atomic emission spectroscopy (model 7510, Shimadzu Co., Kyoto, Japan).

5.4. Relaxivity of conjugated Gd at 7.1 T

Solvent longitudinal relaxation times (T_1) in the aqueous solutions of the gadolinium conjugate were measured at different concentrations of gadolinium conjugate using a mixture of distilled water (0.625%) and deuterium oxide (99.375%) as a solvent. All measurements were performed on a 300 MHz (7.1 T) NMR spectrometer (Gemini2000/300; Varian Inc., CA, USA) using an inversion recovery technique with 19 inversion times (*TI*) ranging from 1 to 5000 ms at ambient temperature (25°C) with a sample concentration of 8 mg per 800 μl. A typical pulse width of 180° pulse was 19 μs. T_1 values were estimated using least-squares fitting of the signal intensities measured at 19 *TI* values in an exponential fashion. The relaxivity of each gadolinium complex was determined by a linear regression of the $1/T_1$ vs the gadolinium complex concentration.

5.5. Cell culture

NIH-3T3 cells were used for evaluating the cytotoxicity, cell labeling potential and imaging efficiency of the Gd–PVA. They were grown in Dulbecco's modified Eagle's medium (DMEM-LG) supplemented with 10% bovine calf serum, 100 units ml^{-1} penicillin, and 100 units ml^{-1} streptomycin at 37°C, 10% CO_2 atmosphere.

5.6. Cytotoxicity assay

NIH-3T3 cells (1×10^4 cells per well) were seeded in a 96-well culture plate and cultured overnight. Varying concentrations (polymer unit concentrations of 10 nM to 10 mM) of **4b** were added to each well. At the indicated time points, the number of cells was measured by WST-1 assay according to the manufacturer's protocol (Takara Shuzo, Otsu, Japan). Briefly, cells were washed with PBS three times, and the culture medium (100 μl) was added to each well. Ten microliters of WST-1 {4-[3-(4-iodophenyl)-2-(4-nitrophenyl)-2H-5-tetrazolio]-1,3-benzene disulfonate} solution was added to each well, and the plates were incubated for 30 min. The absorbance at 450 nm was measured on a microplate reader (Model 550, Bio-Rad Laboratory Co., Tokyo, Japan).

5.7. Cell labeling by electroporation

NIH-3T3 cells were cultured in a 6 cm diameter Petri dish at a concentration of 5×10^5 cells per dish in DMEM-LG for 1 day. An arbitrary amount of **4d** was added to the culture medium, and electrical pulses were applied to cells using a CUY-21 electroporator (CUY-21; NEPPA GENE, Tokyo, Japan). Rectangular electrical pulses (field strength 300 V cm^{-1}, number of pulses 10, pulse duration 5 ms) were applied to cells using two parallel electrodes with a 5 mm gap. Cells were incubated for 1 h and washed with PBS twice.

5.8. Stability of 4d in cells

To determine whether **4d** molecules stay in NIH-3T3 cells for a long period of time, the labeled cells (1×10^4 cells) were seeded in a 6 cm diameter Petri dish and cultured over 10 days without a subculture. The time course of the fluorescence intensity for the cultured cells was measured as follows. Before each measurement, cells in one dish were washed three times with PBS to eliminate the free **4d** from the cells and lysed in 1 ml lysis buffer [25 mM tris (pH 7.8), 2 mM dithiothreitol, 2 mM 1,2-diaminocyclohexan-*N,N,N',N'*-tetraacetic acid, 10% glycerol, 1% Triton X-100]. After 1 h incubation at 37°C, the fluorescence intensity of the cell lysates was measured with a spectrofluorometer (excitation 430 nm, emission 540 nm, Wallac 1420 ARVOsx, Perkin-Elmer Life Sciences, Boston, MA, USA). The time course of the fluorescence intensity represented the stability of **4d** in the cells. At the same time, the number of cells in each dish was counted. In addition, the amount of **4d** delivered into each cell by electroporation was calculated using the standard curve of fluorescence intensity.

5.9. MR imaging of Gd–PVA solution at 4.7 T

MR images of **4d** aqueous solutions were obtained on a 200-MHz (4.7 T) NMR spectrometer (Apollo; Tecmag Inc., TX, USA) equipped with a gradient system (Jeol Ltd, Tokyo, Japan; maximum gradient strength 20 mT m^{-1}; slew late 50 mT m^{-1} ms^{-1}) using a saddle coil with an inner diameter of 47 mm. Aqueous solutions with different concentrations (0.05, 0.1, 0.2, 0.3, 0.5 and 1 mM) of polymer unit were prepared. Three test tubes with different concentrations were fixed vertically. A horizontal section was scanned. T_1-weighted images of the samples were acquired using a 2D spin echo sequence with a repetition time (*TR*) of 2000 ms and an echo time (*TE*) of 16 ms. Taking the long T_1 of the water observed in the 1.5 T machine into account, *TR* was greater in comparison to that for general T_1-weighted images. We used the minimum possible *TE* to minimize the T_2 relaxation effect. Other scanning parameters were as follows: field of view (FOV), 6 × 6 cm; matrix, 256 × 256; slice thickness, 1 cm.

5.10. MR imaging of NIH-3T3 cells *in vitro*

MR measurements of labeled cells were performed using the same scanner and the same parameters as in the imaging of **4d** solutions. Cells labeled with **4d** by electroporation were trypsinized, centrifuged and resuspended in test tubes (75 mm

long, 10 mm in diameter) at 7×10^6 cells in 2 ml of complete DMEM. The test tubes with labeled cell suspensions were allowed to settle for 1 day to allow the cells to be precipitated before MR imaging. A test tube with unlabeled cell suspensions was also prepared in the same manner. In addition, a test tube with cell-free pure medium was prepared. The three test tubes prepared were arranged as shown in Fig. 4(a). Scanned slices were positioned so that they pass through the cell pellet part (slice B in Fig. 4a) or the solution part (slice A in Fig. 4a).

The cell density dependence of signal enhancement was examined as follows. Different numbers of labeled cells were suspended in 100 μl of agarose solution at the concentration of 2 wt% and cooled to be gelated. The MR imaging data of these mixtures were collected by a 1 T compact MR imaging system with a permanent magnet (MRmini, Dainippon Sumitomo Pharma, Osaka, Japan) with a *TE* of 9 ms and a *TR* of 1500 ms (FOV, 3 × 6 cm; matrix, 128 × 256; slice thickness, 3.7 mm).

5.11. *In vivo* fate of free SPIO and free Gd–PVA

The clearance of **4d** and SPIO after intramuscular injection was investigated in male rat F344. The rat was anesthetized by inhalation anesthesia (1.5% isoflurane). Solutions of **4d** (Gd 0.8 μmol per 50 μl water) and carboxydextran-coated SPIO, Resovist™ (Fe 0.8 μmol per 50 μl water, Bayer, Osaka, Japan) were injected into the left and right femoral muscles, respectively, using a 29 G needle. Whole inferior limbs of the animal were scanned at 0, 3 and 10 days after injection on a 1.5 T compact MR imaging system. These images were obtained with a *TR* of 1500 ms and a *TE* of 9 ms (FOV, 4 × 8 cm; matrix, 128 × 256; slice thickness, 1 mm; slice gap, 0 mm; number of slice, 35).

For the time course of the CNR and the number of voxels in the region, whole inferior limbs of the animal were scanned at 0, 1, 4, 6, 8, 11 and 13 days after injection on a 1.5 T compact MR imaging system. These images were obtained with a *TR* of 500 ms and a *TE* of 9 ms, and with a *TR* of 3000 ms and a *TE* of 20 ms (FOV, 4 × 8 cm; matrix, 128 × 256; slice thickness, 1 mm; slice gap, 0 mm; number of slices, 35). CNR was calculated as $(\pi/2)^{1/2}|S_1-S_2|/S_{air}$, where S_1, S_2 and S_{air} were the mean intensities in the contrast-enhanced region, muscle and air, respectively.

5.12. Preliminary MR imaging of transplanted NIH-3T3 cells

In vivo cell tracking was preliminarily performed in male Balb/c mice. These mice were anesthetized for imaging with the use of a general inhalation anesthesia (1.5% isoflurane) and were allowed to breathe spontaneously during preparation and scanning. NIH-3T3 cells labeled with **4d** (2×10^7 cells) were embedded in 2 wt% agarose gel (200 μl) and transplanted to the mice subcutaneously. MR images were obtained using a 2 T compact MR imaging system with a permanent magnet. T_1-weighted images were acquired using a 2D spin echo sequence with a *TR* of 2000 ms and a *TE* of 9 ms (FOV, 3 × 6 cm; matrix, 128 × 256; slice thickness, 1 mm) at room temperature.

6. SUPPORTING INFORMATION

Supporting information can be found in the online version of this article.

Acknowledgements

This work was supported by grants-in-aid from the Ministry of Health, Labour and Welfare of Japan (Health and Labour Sciences Research Grants, Research on Nanotechnical Medical). This work was also supported by a Research Grant for Cardiovascular Diseases (18A-2) from the Ministry of Health, Labour and Welfare of Japan.

References

1. Perin EC, Dohmann HF, Borojevic R, Silva SA, Sousa AL, Mesquita CT, Rossi MI, Carvalho AC, Dutra HS, Dohmann HJ, Silva GV, Belem L, Vivacqua R, Rangel FO, Esporcatte R, Geng YJ, Vaughn WK, Assad JA, Mesquita ET, Willerson JT., Transendocardial, autologous bone marrow cell transplantation for severe, chronic ischemic heart failure. Circulation 2003; 107 18 2294–2302.
2. Schmid C, Schleuning M, Schwerdtfeger R, Hertenstein B, Mischak-Weissinger E, Bunjes D, Harsdorf SV, Scheid C, Holtick U, Greinix H, Keil F, Schneider B, Sandherr M, Bug G, Tischer J, Ledderose G, Hallek M, Hiddemann W, Kolb HJ. Long-term survival in refractory acute myeloid leukemia after sequential treatment with chemotherapy and reduced-intensity conditioning for allogeneic stem cell transplantation. Blood 2006; 108(3): 1092–1099.
3. Slavin S, Nagler A, Naparstek E, Kapelushnik Y, Aker M, Cividalli G, Varadi G, Kirschbaum M, Ackerstein A, Samuel S, Amar A, Brautbar C, Ben-Tal O, Eldor A, Or R. Nonmyeloablative stem cell transplantation and cell therapy as an alternative to conventional bone marrow transplantation with lethal cytoreduction for the treatment of malignant and nonmalignant hematologic diseases. Blood 1998; 91(3): 756–763.
4. Kim SW, Han H, Chae GT, Lee SH, Bo S, Yoon JH, Lee YS, Lee KS, Park HK, Kang KS. Successful stem cell therapy using umbilical cord blood-derived multipotent stem cells for Buerger's disease and ischemic limb disease animal model. Stem Cells 2006; 24(6): 1620–1626.
5. Stamm C, Westphal B, Kleine HD, Petzsch M, Kittner C, Klinge H, Schumichen C, Nienaber CA, Freund M, Steinhoff G. Autologous bone-marrow stem-cell transplantation for myocardial regeneration. Lancet 2003; 361(9351): 45–46.
6. Strauer BE, Brehm M, Zeus T, Kostering M, Hernandez A, Sorg RV, Kogler G, Wernet P. Repair of infarcted myocardium by autologous intracoronary mononuclear bone marrow cell transplantation in humans. Circulation 2002; 106(15): 1913–1918.
7. Grant MB, May WS, Caballero S, Brown GA, Guthrie SM, Mames RN, Byrne BJ, Vaught T, Spoerri PE, Peck AB, Scott EW. Adult hematopoietic stem cells provide functional hemangioblast activity during retinal neovascularization. Nat Med 2002; 8(6): 607–612.
8. Tang YL, Zhao Q, Qin X, Shen L, Cheng L, Ge J, Phillips MI. Paracrine action enhances the effects of autologous mesenchymal stem cell transplantation on vascular regeneration in rat model of myocardial infarction. Ann Thorac Surg 2005; 80(1): 229–236 discussion 236-227.
9. Beeres SL, Bengel FM, Bartunek J, Atsma DE, Hill JM, Vanderheyden M, Penicka M, Schalij MJ, Wijns W, Bax JJ. Role of imaging in cardiac stem cell therapy. J Am Coll Cardiol 2007; 49(11): 1137–1148.
10. Frangioni JV, Hajjar RJ. In vivo tracking of stem cells for clinical trials in cardiovascular disease. Circulation 2004; 110(21): 3378–3383.
11. Tanaka M, Swijnenburg RJ, Gunawan F, Cao YA, Yang Y, Caffarelli AD, de Bruin JL, Contag CH, Robbins RC. In vivo visualization of cardiac allograft rejection and trafficking passenger leukocytes using bioluminescence imaging. Circulation 2005; 112(9 Suppl): I105–110.
12. Wang X, Rosol M, Ge S, Peterson D, McNamara G, Pollack H, Kohn DB, Nelson MD, Crooks GM. Dynamic tracking of human hematopoietic stem cell engraftment using in vivo bioluminescence imaging. Blood 2003; 102(10): 3478–3482.

13. Sutton EJ, Henning TD, Pichler BJ, Bremer C, Daldrup-Link HE. Cell tracking with optical imaging. Eur Radiol 2008; 18(10): 2021–2032.
14. Takagi Y, Takahashi J, Saiki H, Morizane A, Hayashi T, Kishi Y, Fukuda H, Okamoto Y, Koyanagi M, Ideguchi M, Hayashi H, Imazato T, Kawasaki H, Suemori H, Omachi S, Iida H, Itoh N, Nakatsuji N, Sasai Y, Hashimoto N. Dopaminergic neurons generated from monkey embryonic stem cells function in a Parkinson primate model. J Clin Invest 2005; 115(1): 102–109.
15. Takahashi M, Nakamura T, Toba T, Kajiwara N, Kato H, Shimizu Y. Transplantation of endothelial progenitor cells into the lung to alleviate pulmonary hypertension in dogs. Tissue Eng 2004; 10(5–6): 771–779.
16. Tomita S, Mickle DA, Weisel RD, Jia ZQ, Tumiati LC, Allidina Y, Liu P, Li RK. Improved heart function with myogenesis and angiogenesis after autologous porcine bone marrow stromal cell transplantation. J Thorac Cardiovasc Surg 2002; 123(6): 1132–1140.
17. Kraitchman DL, Tatsumi M, Gilson WD, Ishimori T, Kedziorek D, Walczak P, Segars WP, Chen HH, Fritzges D, Izbudak I, Young RG, Marcelino M, Pittenger MF, Solaiyappan M, Boston RC, Tsui BM, Wahl RL, Bulte JW. Dynamic imaging of allogeneic mesenchymal stem cells trafficking to myocardial infarction. Circulation 2005; 112(10): 1451–1461.
18. Hill JM, Dick AJ, Raman VK, Thompson RB, Yu ZX, Hinds KA, Pessanha BS, Guttman MA, Varney TR, Martin BJ, Dunbar CE, McVeigh ER, Lederman RJ. Serial cardiac magnetic resonance imaging of injected mesenchymal stem cells. Circulation 2003; 108(8): 1009–1014.
19. Rice HE, Hsu EW, Sheng H, Evenson DA, Freemerman AJ, Safford KM, Provenzale JM, Warner DS, Johnson GA. Superparamagnetic iron oxide labeling and transplantation of adipose-derived stem cells in middle cerebral artery occlusion-injured mice. AJR Am J Roentgenol 2007; 188(4): 1101–1108.
20. Stuckey DJ, Carr CA, Martin-Rendon E, Tyler DJ, Willmott C, Cassidy PJ, Hale SJ, Schneider JE, Tatton L, Harding SE, Radda GK, Watt S, Clarke K. Iron particles for noninvasive monitoring of bone marrow stromal cell engraftment into, and isolation of viable engrafted donor cells from, the heart. Stem Cells 2006; 24(8): 1968–1975.
21. Hoshino K, Ly HQ, Frangioni JV, Hajjar RJ. In vivo tracking in cardiac stem cell-based therapy. Prog Cardiovasc Dis 2007; 49(6): 414–420.
22. Amsalem Y, Mardor Y, Feinberg MS, Landa N, Miller L, Daniels D, Ocherashvilli A, Holbova R, Yosef O, Barbash IM, Leor J. Iron-oxide labeling and outcome of transplanted mesenchymal stem cells in the infarcted myocardium. Circulation 2007; 116(11 Suppl): I38–45.
23. Li Z, Suzuki Y, Huang M, Cao F, Xie X, Connolly AJ, Yang PC, Wu JC. Comparison of reporter gene and iron particle labeling for tracking fate of human embryonic stem cells and differentiated endothelial cells in living subjects. Stem Cells 2008; 26(4): 864–873.
24. Yamaoka T, Tabata Y, Ikada Y. Comparison of body distribution of poly(vinyl alcohol) with other water-soluble polymers after intravenous administration. J Pharm Pharmacol 1995; 47(6): 479–486.
25. Walczak P, Kedziorek DA, Gilad AA, Lin S, Bulte JW. Instant MR labeling of stem cells using magnetoelectroporation. Magn Reson Med 2005; 54(4): 769–774.
26. Pillai O, Panchagnula R. Polymers in drug delivery. Curr Opin Chem Biol 2001; 5(4): 447–451.
27. Li TS, Hamano K, Suzuki K, Ito H, Zempo N, Matsuzaki M. Improved angiogenic potency by implantation of ex vivo hypoxia prestimulated bone marrow cells in rats. Am J Physiol Heart Circ Physiol 2002; 283(2): H468–473.
28. Zhang S, Ge J, Zhao L, Qian J, Huang Z, Shen L, Sun A, Wang K, Zou Y. Host vascular niche contributes to myocardial repair induced by intracoronary transplantation of bone marrow CD34+ progenitor cells in infarcted swine heart. Stem Cells 2007; 25(5): 1195–1203.
29. Oude Engberink RD, van der Pol SM, Dopp EA, de Vries HE, Blezer EL., Comparison of SPIO and USPIO for in vitro labeling of human monocytes: MR detection and cell function. Radiology 2007; 243(2): 467–474.
30. Aime S, Cabella C, Colombatto S, Geninatti Crich S, Gianolio E, Maggioni F. Insights into the use of paramagnetic Gd(III) complexes in MR-molecular imaging investigations. J Magn Reson Imag 2002; 16(4): 394–406.
31. Gustafsson B, Youens S, Louie AY. Development of contrast agents targeted to macrophage scavenger receptors for MRI of vascular inflammation. Bioconjug Chem 2006; 17(2): 538–547.
32. Langereis S, de Lussanet QG, van Genderen MH, Meijer EW, Beets-Tan RG, Griffioen AW, van Engelshoven JM, Backes WH. Evaluation of Gd(III)DTPA-terminated poly(propylene imine) dendrimers as contrast agents for MR imaging. NMR Biomed 2006; 19(1): 133–141.
33. Lu ZR, Wang X, Parker DL, Goodrich KC, Buswell HR. Poly(-l-glutamic acid) Gd(III)–DOTA conjugate with a degradable spacer for magnetic resonance imaging. Bioconjug Chem 2003; 14(4): 715–719.
34. Nakamura E, Makino K, Okano T, Yamamoto T, Yokoyama M. A polymeric micelle MRI contrast agent with changeable relaxivity. J Control Release 2006; 114(3): 325–333.
35. Wen X, Jackson EF, Price RE, Kim EE, Wu Q, Wallace S, Charnsangavej C, Gelovani JG, Li C. Synthesis and characterization of poly(L-glutamic acid) gadolinium chelate: a new biodegradable MRI contrast agent. Bioconjug Chem 2004; 15(6): 1408–1415.
36. Yan GP, Liu ML, Li LY. Polyaspartamide gadolinium complexes containing sulfadiazine groups as potential macromolecular MRI contrast agents. Bioconjug Chem 2005; 16(4): 967–971.
37. Yamaoka T, Tabata Y, Ikada Y. Distribution and tissue uptake of poly(ethylene glycol) with different molecular weights after intravenous administration to mice. J Pharm Sci 1994; 83(4): 601–606.
38. Yamaoka T, Tabata Y, Ikada Y. Fate of water-soluble polymers administered via different routes. J Pharm Sci 1995; 84(3): 349–354.

Timing-controlled Decompaction of Polyplexes In Vivo Greatly Enhances Transgene Expression

Yoichi Tachibana,[1] Tomoko Hashimoto,[1,2] Hisae Nozaki,[1] Akira Murakami,[2] and Tetsuji Yamaoka[1]
[1]*Department of Biomedical Engineering, National Cerebral and Cardiovascular Center Research Institute, Fujishirodai, Suita, Osaka 565-8585*
[2]*Department of Biomolecular Engineering, Kyoto Institute of Technology, Matsugasaki, Sakyo-ku, Kyoto 606-8585*

(Received September 8, 2010; CL-100773; E-mail: yamtet@ri.ncvc.go.jp)

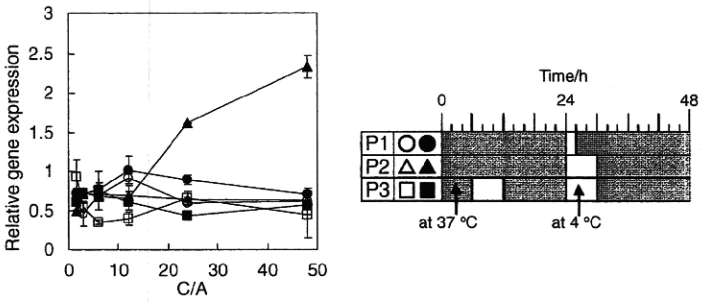

REPRINTED FROM
Chemistry Letters

Vol.39 No.12 2010 p.1238–1239
CMLTAG
December 5, 2010

The Chemical Society of Japan

Published on the web October 23, 2010; doi:10.1246/cl.2010.1238

doi:10.1246/cl.2010.1238
1238 Published on the web October 23, 2010

Timing-controlled Decompaction of Polyplexes In Vivo Greatly Enhances Transgene Expression

Yoichi Tachibana,[1] Tomoko Hashimoto,[1,2] Hisae Nozaki,[1] Akira Murakami,[2] and Tetsuji Yamaoka[1]
[1]*Department of Biomedical Engineering, National Cerebral and Cardiovascular Center Research Institute, Fujishirodai, Suita, Osaka 565-8585*
[2]*Department of Biomolecular Engineering, Kyoto Institute of Technology, Matsugasaki, Sakyo-ku, Kyoto 606-8585*

(Received September 8, 2010; CL-100773; E-mail: yamtet@ri.ncvc.go.jp)

Compaction extent of polyplexes was successfully regulated by cold treatment in buffer solution using thermoresponsive gene carriers composed of linear poly(ethyleneimine) (l-PEI) and alkyl side chains. Plasmid DNA (pCMV-Luc) was transfected to COS-1 cells using these carriers with different cold treatments. The luciferase expression was greatly enhanced when cells were treated at 4 °C in well-defined timing. This was a direct observation of how intracellular destabilization in regulated timing is important for nonviral gene transfection.

There has been significant interest in synthetic polycation as a non-viral gene carrier and in gene therapy.[1] Several polycationic carriers, such as poly(ethyleneimine) (PEI),[2] poly(L-lysine) (PLL),[3] and chitosan,[4] have been developed due to various advantages over viral vectors. Among them, PEI is one of the most widely studied gene carriers because of its high efficiency gene expression.[2] Furthermore, mechanism analysis for efficient gene transfer including cellular uptake, lysosomal escape, and nuclear transport has been widely carried out. Although the decompaction or dissociation of polyplexes is believed to be important for gene expression, studies of this are not well developed because it is not easy to control these phenomena in cells.

Recently, thermoresponsive polymers have received much attention as intelligent materials for various applications. Poly(*N*-isopropylacrylamide) (PNIPAAm) is one of the most typical thermoresponsive polymers.[5] A block copolymer consisting of poly(L-lactic acid) and poly(ethylene glycol)[6] and poly(amino acid)s[7] have been also reported. Kurisawa et al. reported that thermoresponsive copolymer, poly[*N*-isopropylacrylamide-*co*-2-(dimethylamino)ethyl methacrylate-*co*-butyl methacrylate], showed high transfection efficiency.[8,9] A PEI-*graft*-PNIPAAm copolymer was synthesized as a thermoresponsive carrier by Bisht et al.[10] Lavigne et al. reported that high gene expression using PEI–PNIPAAm conjugates as a carrier occurred below the LCST.[11] We report herein synthesis and timing-controlled gene transfection by use of new thermoresponsive PEI derivatives as gene carriers. PEI derivatives were synthesized by the reaction of l-PEI ($M_w = 22000$) with various carboxylic acid chlorides in chloroform at room temperature for 48 h (Scheme 1). In this study, butyryl chloride, propanoyl chloride, and hexanoyl chloride were used for the synthesis of PEI derivatives. The synthesis of PEI derivatives is summarized in Table 1 and the introduction ratio was determined by ^{1}H NMR. PEI-C4 was soluble in water at room temperature. PEI-C5 and PEI-C6 were insoluble in water.

Figure 1 shows the transfection efficiency of PEI derivative/pCMV-Luc complexes. Complexes were formed by mixing PEI derivatives with pCMV-Luc at several cation/anion (C/A) ratios. The transfection efficiency was determined by luciferase activity in COS-1 cells at 37 °C. PEI homopolymer as a control showed high transfection efficiency with increasing C/A ratio. The transfection efficiency of PEI-C4 at high C/A ratios of 24 and 48 was almost the same as that of PEI. It was demonstrated that the transfection efficiency was not affected by the introduction into the side chain of PEI. For PEI-C5 and PEI-C6, low transfection efficiencies were observed because of their low solubility in water.

Figure 2 shows photographs of 1 wt% solution of PEI-C4 at 4 and 37 °C. The transparent solution at 4 °C became opaque at 37 °C. The turbidity change took place sharply in both heating and cooling processes. This result showed that PEI-C4 was

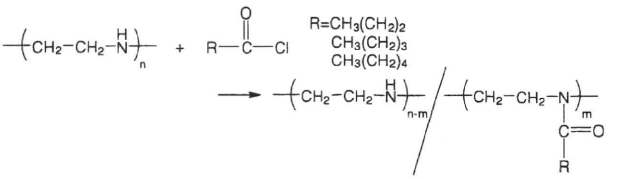

Scheme 1.

Table 1. Synthesis of PEI derivatives

Sample	Chloride	Yield/%	Introduction ratio[a]/%
PEI-C4	Butyryl chloride	55	64
PEI-C5	Propanoyl chloride	64	67
PEI-C6	Hexanoyl chloride	59	58

[a]Determined by ^{1}H NMR.

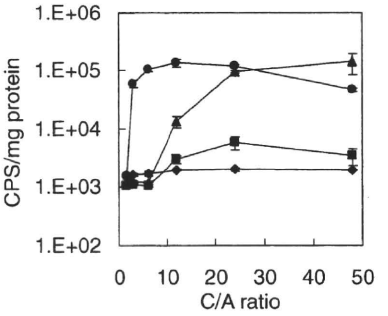

Figure 1. Transfection efficiency determined by luciferase activity in COS-1 at 37 °C. The polyplexes composed of pCMV-Luc (100 ng) and polycations (C/A 48–1.5) in FBS (−) DMEM were added to culture medium for 1×10^4 cells per well in the presence of 100 μM chloroquine. ●: PEI, ▲: PEI-C4, ■: PEI-C5, and ◆: PEI-C6. Values are shown as means ± standard deviations.

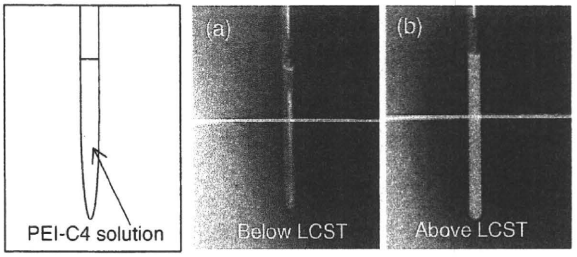

Figure 2. Photographs of the 1 wt% polymer solution of PEI-C4 at (a) 4 and (b) 37 °C.

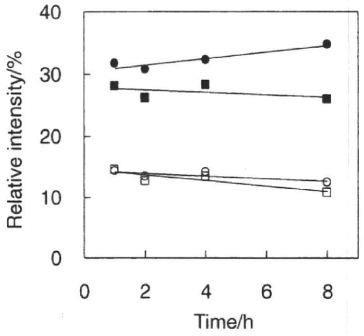

Figure 3. Relative fluorescence intensities of complexes depending on the temperature. Fluorescein-labeled plasmid DNA was complexed with PEI or PEI-C4. Complexes were incubated at 4 or 37 °C for various times. ●: PEI-C4 (4 °C), ■: PEI-C4 (37 °C), ○: PEI (4 °C), and □: PEI (37 °C).

thermoresponsive polymer. The LCST of PEI-C4 was estimated around 30 °C.

Relative fluorescence intensities of complexes depending on the temperature were examined (Figure 3). Fluorescein-labeled pCMV-Luc (F-pCMV-Luc) was complexed with PEI or PEI-C4 at the C/A ratio of 24 and complexes were incubated at 4 or 37 °C for 1, 2, 4, and 8 h. A gradual increase in the relative fluorescence intensity of PEI-C4/F-pCMV-Luc complex by treating at 4 °C was found, whereas such increase was not observed when the complex was incubated at 37 °C. In the case of PEI, the change of relative fluorescence intensities was not observed. This change must be because of the decompaction of the polyplexes resulting from the increased hydrophilicity of the PEI-C4. The temperature lower than the LCST caused a conformational change of PEI-C4 and made the complex unstable.

Effects of the post-transfection cold procedure on the luciferase expression are shown in Figure 4B. Relative gene expression was calculated as follows: (CPS/mg protein with the cooling procedure)/(CPS/mg protein without the cooling procedure). When cells were treated at 4 °C for 6 h at 24 h post transfection, the relative gene expression increased 2.3 times (Figure 4A, ▲). This kind of enhancement was not observed for the PEI (Figure 4A, open marks). The cold treatment for 2 h did not affect the expression at all (Figure 4A, ●). This may be due to insufficient decompaction of the polyplexes. The internalized complexes are considered to be decompacted as is shown in Figure 3 and were transcribed, resulting in high gene expression. When cells were cold treated for 6 h at 6 h post transfection, the

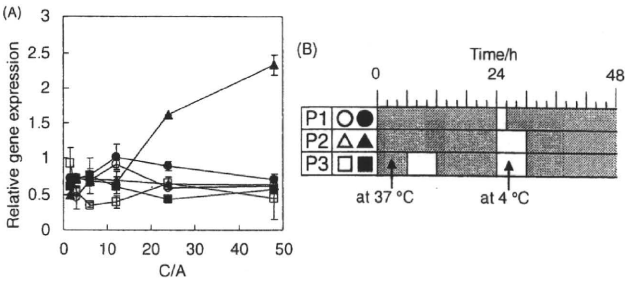

Figure 4. Relative gene expression depending on temperature (A). Cells were incubated with complexes composed of pCMV-Luc (100 ng) and polycations (C/A 48–1.5) in FBS (−) DMEM. PEI-C4 (closed symbol) and PEI (open symbol) were used. The cooling procedure is shown on panel B.

expression enhancement was not observed even for the 6 h cold treatment at 24 h post transfection (Figure 4A, ■), suggesting that the decompaction at a too early stage in the intracellular trafficking of polyplexes suppressed the gene expression completely.

In conclusion, new thermoresponsive polymers based on PEI were used for controlling the intracellular decompaction of the polyplexes. Thermoresponse was found in polymer solution prepared by the reaction of butyryl chloride with PEI. The stability of PEI-C4/F-pCMV-Luc complex was clearly affected by cold treatment in a buffer solution. Furthermore, high gene expression was achieved by well-defined cold treatment procedure. Our system will be useful for mechanistic analysis of the intracellular behavior of polyplexes for efficient polymeric carrier-based gene transfer.

This work was supported by Grants-in-Aid from the Ministry of Health, Labour and Welfare of Japan and by the Program for Promotion of Fundamental Studies in Health Sciences of National Institute of Biomedical Innovation of Japan.

References

1 a) A. V. Kabanov, V. A. Kabanov, *Bioconjugate Chem.* **1995**, *6*, 7. b) T. Hashimoto, Y. Tachibana, H. Nozaki, O. Mazda, T. Niidome, A. Murakami, T. Yamaoka, *Chem. Lett.* **2009**, *38*, 718.
2 W. T. Godbey, K. K. Wu, A. G. Mikos, *J. Controlled Release* **1999**, *60*, 149.
3 V. Toncheva, M. A. Wolfert, P. R. Dash, D. Oupicky, K. Ulbrich, L. W. Seymour, E. H. Schacht, *Biochim. Biophys. Acta* **1998**, *1380*, 354.
4 T. H. Kim, I. K. Park, J. W. Nah, Y. J. Choi, C. S. Cho, *Biomaterials* **2004**, *25*, 3783.
5 M. Heskins, J. E. Guillet, *J. Macromol. Sci., Part A: Pure Appl. Chem.* **1968**, *2*, 1441.
6 T. Fujiwara, T. Mukose, T. Yamaoka, H. Yamane, S. Sakurai, Y. Kimura, *Macromol. Biosci.* **2001**, *1*, 204.
7 a) Y. Tachibana, M. Kurisawa, H. Uyama, T. Kakuchi, S. Kobayashi, *Chem. Commun.* **2003**, 106. b) Y. Tachibana, M. Kurisawa, H. Uyama, S. Kobayashi, *Biomacromolecules* **2003**, *4*, 1132.
8 B. R. Twaites, C. de las Heras Alarcón, D. Cunliffe, M. Lavigne, S. Pennadam, J. R. Smith, D. C. Górecki, C. Alexander, *J. Controlled Release* **2004**, *97*, 551.
9 a) M. Kurisawa, M. Yokoyama, T. Okano, *J. Controlled Release* **2000**, *68*, 1. b) M. Kurisawa, M. Yokoyama, T. Okano, *J. Controlled Release* **2000**, *69*, 127. c) M. Yokoyama, M. Kurisawa, T. Okano, *J. Artif. Organs* **2001**, *4*, 138.
10 H. S. Bisht, D. S. Manickam, Y. You, D. Oupicky, *Biomacromolecules* **2006**, *7*, 1159.
11 M. D. Lavigne, S. S. Pennadam, J. Ellis, L. L. Yates, C. Alexander, D. C. Górecki, *J. Gene Med.* **2007**, *9*, 44.

第2章 先端科学技術とDDS開発

1 医用工学とDDS

DDS for Biomedical Engineering

国立循環器病センター研究所 先進医工学センター 生体工学部
山岡哲二
TETSUJI YAMAOKA
Department of Biomedical Engineering, Advanced Medical Engineering Center, National Cardiovascular Center Research Institute

はじめに

医用工学に関する多くの学会では，人工臓器や生体材料のセッションに加えてDDS関連のセッションが設けられている。DDS研究は，工学者にとっても魅力的な領域であり，いろいろなDDS用材料群や新たなシステムが開発研究されてきた。医薬品は，広義には「身体の構造または機能に影響を及ぼすことが目的とされているものであって，機械器具などではないもの」であり，医療機器と区別されているようであるが，近年，これらは急激に接近して，その境界はもはや明確ではない。また，分子生物学・再生医工学の進歩とともに，さまざまなタンパク製剤やホルモン製剤，あるいはさまざまな生体由来シグナル分子が医薬品となり，さらに，機能細胞までもが「身体の機能に影響をおよぼすもの」として捉えられる時代が始まった。本稿では，医療機器研究の立場から，DDSあるいは医薬品との今後の関わりについて考えたい。

1．機能性医療機器

薬事法は，医薬品だけではなく，医薬部外品，化粧品，そして，医療機器も規制している。昭和23年に作られた「新たな薬事法」から長い年月を経て，平成17年に改正薬事法が実施された。それに伴い，医療用具は医療機器と改名されている。一口に医療機器と言っても，医療現場で使うピンセット，注射針からMRI，そして，マッサージチェアまでが，薬事法で規制される医療機器である。医療機器開発は，医薬品開発・DDS研究と協同的に歩んできた。非分解性の人工弁・人工心臓・人工血管などの抗血栓性は完全なものではなく，医薬品投与とDDS技術導入によりサポートされ，また，生体活性分子を用いた表面修飾によっても，さらなる機能化が施されてきた（**図1**）。近年，薬物放出ステント（DES：Drug-Eluting Stent）に代表されるように直接的に融合した医療機器の出現に伴い，両者の境界はますます見えにくくなっている。

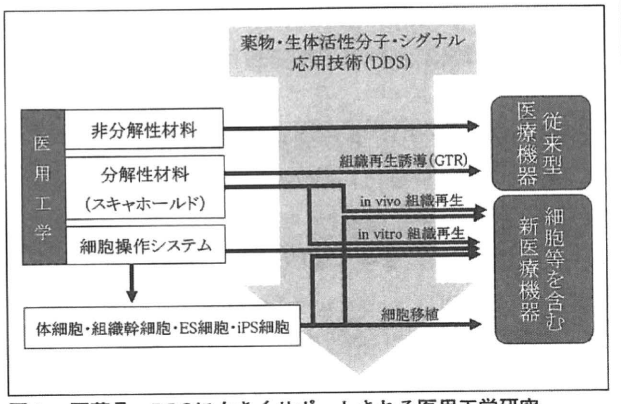

図1　医薬品・DDSに大きくサポートされる医用工学研究

(1) ステント

ステント適応後の再狭窄防止を目的に，再狭窄抑止効果のある薬物を徐放するDESは，2004年に輸入承認されて国内販売が始まった。同年のDESの市場は約160億円で，翌年には約600億円にまで達した[1]。現在のDESには，

主に，細胞増殖抑制を作用機序とするパクリタキセル系，および，免疫抑制を主な作用機序とするシロリムス系が用いられている。システムとしてはDDSデバイスのようにも感じられるが，承認は医療機器であり，融合デバイスの象徴的存在である。近年の，ステントの全市場が900億円程度であることから，その中のDESのシェアは75%にものぼる。一方で，2006年米国心臓学会で，遅発性ステント血栓症(LST：Late Stent Thrombosis)の発症率がDES適応例で有意に高いことが示され，現在も，その有効性と安全性が議論されていることもあり，このシェアに動きが出始めている。LSTのメカニズムはいまだ解明されていないが，薬物放出担体としてステント表面にコーティングされているマトリックス材料に対する長期炎症のために，一度構築された内皮層が遅発性に損傷を受けることによるとの危惧もあり，新規材料に対する研究開発が精力的に進んでいる。まさに研究開発においても，医療機器開発とDDS研究との融合が必須である。

(2)生理活性分子による医療機器の機能化

同様の目的のために，2005年には，表面に抗CD34抗体をコーティングしたステントの臨床研究成果が発表された[2]。末梢血中に存在するCD34陽性細胞である血管内皮前駆細胞(EPC：Endotherial Progenitor Cell[3])がステント表面に結合して，内皮化促進につながることを狙った新規デバイスである。さらに，翌年には，インテグリン接着性細胞接着因子であるRGDトリペプチドをコーティングしたステントにおいてもEPCのリクルートメントが誘導できるとの臨床研究が報告されている[4]。抗CD34抗体もRGDトリペプチドも，まさに「身体の機能に影響をおよぼすもの」として捉えることができる。

われわれは，再生型人工血管の臨床研究で優れた実績を有する東京女子医科大学の研究グループ[5]と共同で，ポリ乳酸／ポリカプロラクトン共重合体多孔質人工血管に対する抗CD34抗体の固定化を検討してきた[6]。すなわち，抗CD34抗体修飾した生体吸収性人工血管に対してCD34陽性の造血幹細胞あるいはEPCをリクルートする治療システムの構築を目指した(**図2**)。すでに，東京女子医大にて血管再生用スキャホールドとして用いられているポリ乳酸の多孔質体の表面を，所定濃度のNaOHで加水分解することで表面にカルボキシル基を導入し，カルボジイミド法により，抗CD34抗体を固定化した。この抗体修飾スキャホールド上に，CD34陽性細胞，CD34陰性細胞，および，イヌ骨髄細胞を約2×10^6個/50mlの濃度で，流速0.05ml/minで播種し，接着した細胞数を計数して免疫染色にて評価したところ，抗体固定化スキャホールド上には，陽性／陰性混合細胞系では80%程度のCD34陽性細胞濃縮効率が得られ，イヌ骨髄細胞播種システムでは約4倍のCD34陽性細胞が認められた。このような，生理活性分子により修飾された医療機器の機能性は，生理活性分子の固定化や徐放化と大きく関連し，人工骨や人工皮膚，神経誘導管など多くの再生医療用医療機器で今後検討が進むと考えられ得る。

2．再生医療の進歩とともに

米国において始まったTissue Engineering(組織工学)研究は，大きな損傷を受けた組織や臓器を修復でき，さらに，組織移植や人工臓器の欠点を補う新たな治療法として注目された。1993年，R. Langerらは，スキャホールド(Scaffold，足場材料)と呼ばれたポリグリコール酸

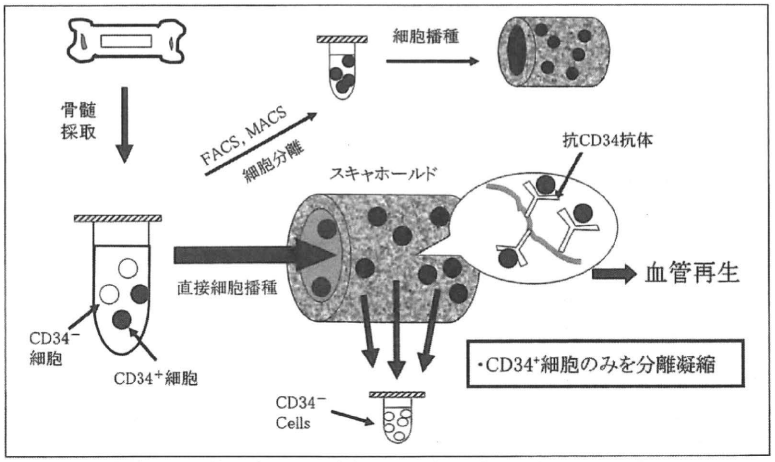

図2　幹細胞特異的抗体を表面に固定化した血管再建用スキャホールド

(PGA)の不織布に軟骨細胞を播種してヌードマウスの皮下に埋入することで，異所的な軟骨の再生が誘導できることを示唆した[7]。その後，わが国においては，2007年10月にヒト自家移植組織(ジェイス™)が，わが国初のヒト細胞を含む医療機器としての製造承認を得た[8]。実は，このようなマトリックスと細胞とを融合させるアイデアは古くから検討され，基礎技術の確立から30年の時を経ての実用化である。これらの新たな医療機器においては，今後も，薬物や細胞とマトリックスとの融合技術がボトルネックとなる(図1)。

細胞を用いた医療機器開発において，機能細胞の安定な調製は困難を極めたが，1981年にマウス胚性幹細胞が[9,10]，さらに1998年には，ヒト胚性幹細胞の単離が報告され[11]，allogeneicな体細胞の入手が可能になると期待された。その後，2007年には山中らがヒトiPS細胞(induced Pluripotent Stem Cell)を発表することで，autologousな体細胞の入手までもが可能な状況となりつつある。そのため，最も単純かつ，早期の臨床化が期待される再生医療の系として，細胞移植療法が精力的に検討され，心筋梗塞[12,13]や下肢虚血，筋萎縮性側索硬化症[14]に対する基礎検討から，臨床成果に至る多くの報告がなされている。このような状況のもと，組織の治癒力を利用した組織再生に直接的に作用すると期待されるのが増殖因子[15]であり，さまざまな投与システムによる効果増強に期待がもたれる[16]。ここでは，変遷を続ける今後の再生医療を支援するための物質送達システムのわれわれの取り組みについて2点紹介したい。

(1)インジェクタブルスキャホールド

これまで述べてきたように，従来の薬物のみならず，タンパク質やシグナル分子，さらには，細胞やその集合体としての小さな組織までが「身体の機能に影響をおよぼすもの」として利用され始め，今後のDDSは，薬物を送達するのみならず，細胞や組織をも送達する必要がある。例えば，幹細胞の懸濁液を直接心筋組織に注入した場合には，細胞の生着率は極めて低い。そこで，細胞注入を支援する材料として，体内で，水溶液から含水ゲルへ相転移する生体吸収性材料(インジェクタブルスキャホールド)が注目されている。2003年バイオマテリアル誌に，“Injectable Polymeric Material”という特集が組まれ，体内でゲル化する材料の有用性が提唱された。当時，光反応性基や，化学反応性基，あるいは，ポリ(N-イソプロピルアクリルアミド)などの温度応答性ポリマーが利用されたが，いずれもその生体内での安全性は確保されていない。われわれは，京都工芸繊維大学木村良晴教授らと共同で研究を進め[17]，PLAとポリエチレングリコール(PEG)という，生体内での利用実績に優れる2つの高分子材料のみを利用することで，温度応答性を実現させインジェクタブルスキャホールドとすることに成功した。

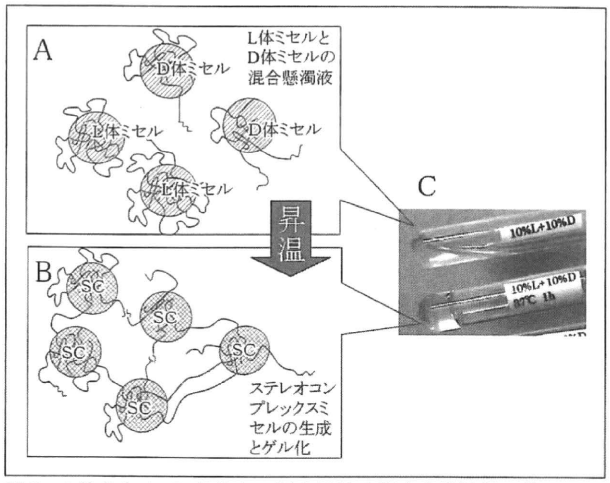

図3　L体ミセル／D体ミセル混合溶液の温度応答性ゲル化

そのゲル化メカニズムを**図3**に示した。ポリエチレングリコール-ポリ乳酸-ポリエチレングリコールという構造のトリブロック共重合体は，水溶液中でナノミセルを形成する。そこで，ポリ-L-乳酸からなるミセル(L体ミセル)と，ポリ-D-乳酸からなるミセル(D体ミセル)の分散液を混合する(図3A)。この溶液を加熱すると，隣接するL体ミセルとD体ミセルが融合し，ステレオコンプレックスミセル(SCミセル)が形成する。すなわち，L体結晶とD体結晶が融合し，新たに融点が約50℃も高い安定なSC結晶を生成する。このことにより，架橋剤や感温性分子を使うことなく，温度応答性のゲル化が可能となった。実際に，共重合組成などを調節して37℃でゲル化することに成功したインジェクタブルスキャホールドの写真を図3Cに示した。X線散乱測定により，温度上昇とともにステレオコンプレックス結晶が成長することがそのメカニズムであることも証明された。得られたゲルの含水率は90%以上であり，その物質透過性に優れた。さらに，緑色蛍光タンパク(GFP)組換え細胞の移植実験により，細胞生存率を下げることなく，また，ゲル内での長期細胞生存を可能にする物質透過性を有し，対象部位に細胞を注入できる材料であることが，明らかとなっている。

(2)幹細胞トラッキング

もう1つの課題は，送達した細胞成分の*in vivo*での動態が不明なことである。特に自己細胞移植では移植細胞を区別して観察することは容易ではなく，移植による治癒メカニズムも解明されていない。1つの手法として，GFP陽性細胞をGFP陰性マウスに移植して*in vivo*蛍光イメージング装置で追跡する手法があるが，蛍光の特性により，ラット程度の小動物が限界である。最近，われわれは移植した細胞をMRIで低侵襲的に追跡するための，新たな細胞標識用MRI造影剤の開発に成功した。**図4**に本システムの概要を示した。ガドリニウム錯体分子(丸印)の細胞膜透過性を抑制し，かつ，細胞に対する毒性を軽減させるために高分子キャリアーを用い，微弱な電気的ショックを細胞に加える手法により，あらゆる細胞に対して容易に送達することに成功した[18]。NIH3T3細胞，およびラット間葉系幹細胞，ラットEPCを標識したところ，その細胞増殖性は非標識細胞と同程度であり，その分化能力も維持されており，さらに，30日間にわたる観察でも造影剤の漏出は認められなかった。ラット下肢虚血モデルラットに移植したEPCが虚血部位へとマイグレートしている挙動がMR撮像によりとらえられている。また，細胞移植による肉腫生成も低侵襲的に追跡できる可能性が示唆されており，現在，詳細な細胞トラッキング解析を進めている。本造影剤で移植細胞数や移植回数を最低限に抑えることで，リスク回避と治療効果の最適化が可能になればと期待している。

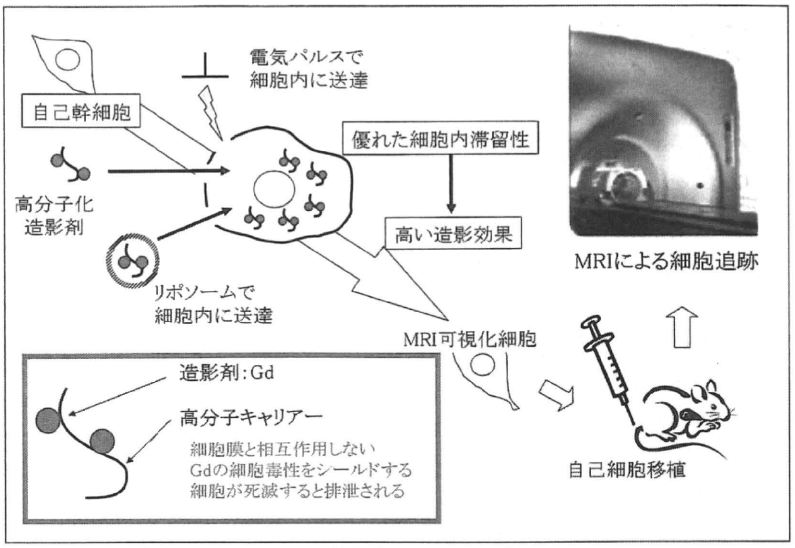

図4 Gd系水溶性MR造影剤による幹細胞トラッキング

■引用文献
1) 医療機器・用品年間2008年版(株式会社アールアンドディ)
2) J. Aoki, P.W. Serruys, H. van Beusekom, A.T.L. Ong, E.P. McFadden, G.S. Willem, J. van der Giessen, E. Regar, P.J. de Feyter, H.R. Davis, S. Rowland, M.J.B. Kutryk：J Am. College Cardiol. **45**(10), (2005)
3) T. Asahara, T. Murohara, A. Sullivan, M. Silver, R. Van Der Zee, T. Li, B. Witzenbichler, G. Schatteman, J.M. Isner：Science, **275**, 964-967(1997)
4) R. Blindt, F. Vogt, I. Astafieva, C. Fach, M. Hristov, N. Krott, B. Seitz, A. Kapurniotu, C. Kwok, M. Dewor, A-K. Bosserhoff, J. Bernhagen, P. Hanrath, R. Hoffmann, C. Weber：J Am College Cardiol., **47**(9)(2006)
5) G. Matsumura, S. Miyagawa-Tomita, T. Shin'oka, Y. Ikada, H. Kurosawa：Circulation, **108**(14), 1729-34(2003)
6) 再生医療用支持体，血管再生用支持体，神経再生用支持体及び治療方法, 特願2003-412423
7) R. Langer, J.P. Vacanti, Science, **260**, 920-926(1993)
8) http://www.jpte.co.jp/Professional/JACE/index.html
9) M.J. Evans, M.H. Kaufman：Nature, **292**, 154-156(1981)
10) G.R. Martin：PNAS, **78**, 7634-7638(1981)
11) J.A. Thomson：Science, **282**, 1145-1147(1998)
12) I.A. Memon, Y. Sawa, N. Fukushima, G. Matsumiya, S. Miyagawa, S. Taketani, S. K. Sakakida, H. Kondoh, A. N. Aleshin, T. Shimizu, T. Okano, H. Matsuda：J Thor. Cardiovasc. Surg., **130**(5), 1333-1341(2005)
13) Y. Miyahara, N. Nagaya, M. Kataoka, B. Yanagawa, K. Tanaka, H. Hao, K. Ishino, H. Ishida, T. Shimizu, K. Kangawa, S. Sano, T. Okano, S. Kitamura, H. Mori：Nature Medicine, **12**, 459-465(2006)
14) L. Mazzini, I. Ferrero, V. Luparello, D. Rustichelli, M. Gunetti, K. Mareschi, L. Testa, A. Stecco, R. Tarletti, M. Miglioretti, E. Fava, N. Nasuelli, C. Cisari, M. Massara, R. Vercelli, G.D. Oggioni, A. Carriero, R. Cantello, F. Monaco, F. Fagioli：Exper. Neurol. on line(2009)
15) S. Akita, K. Akino, T. Imaizumia, A. Hirano, Burns, **31**, 855-858(2005)
16) Babensee, J.E.a, McIntire, L.V.b , Mikos, A.G.b Pharmaceutical Research：**17**, 497-504(2000)
17) T. Fujiwara, T. Mukose, T. Yamaoka, H. Yamane, S. Sakurai, Y. Kimura：Macromol. Biosci., **1**, 204-208(2001)
18) Y. Tachibana, J. Ennmi, H. Iida, T. Yamaoka, Abstract for SFB 2007 Annual meeting, **94**(2007)

3-Tesla Magnetic Resonance Angiographic Assessment of a Tissue-Engineered Small-Caliber Vascular Graft Implanted in a Rat

Masashi Yamanami,[1,2] Akihide Yamamoto,[3,4] Hidehiro Iida,[3,4] Taiji Watanabe,[1,2] Keiichi Kanda,[2] Hitoshi Yaku,[2] Yasuhide Nakayama[1]

[1] Department of Bioengineering, Advanced Biomedical Engineering Center, National Cardiovascular Center Research Institute, Osaka, Japan

[2] Department of Cardiovascular Surgery, Kyoto Prefectural University of Medicine, Kyoto, Japan

[3] Department of Investigative Radiology, Advanced Biomedical Engineering Center, National Cardiovascular Center Research Institute, Osaka, Japan

[4] Department of Medical Physics and Engineering, Division of Health Sciences, Graduate School of Medicine, Osaka University, Osaka, Japan

Received 30 January 2009; revised 4 June 2009; accepted 15 July 2009
Published online 2 October 2009 in Wiley InterScience (www.interscience.wiley.com). DOI: 10.1002/jbm.b.31501

Abstract: In the development of small-caliber vascular grafts (diameter; less than 3 mm), animal implantation studies have been mostly performed by using rat abdominal aortas, and their certain patency must evaluate with sacrificing every observation periods, which is both labor-intensive and time-consuming when performing a large number of experiments. This study is the first to demonstrate the application of 3-Tesla contrast-free time-of-flight magnetic resonance angiography (TOF-MRA) in the continuous assessment of the status of a tissue-engineered vascular graft in rat. As a model graft, a single connective tubular tissue (diameter; 1.5 mm), prepared by embedding the silicone rod (diameter; 1.5 mm) into a subcutaneous pouch of a rat for 2 weeks an *in vivo* tissue-engineering, was used. The graft was implanted in the abdominal aorta (diameter; 1.3 mm) of the rat by end-to-end anastomosis. Repeated TOF-MRA imaging of the graft obtained over a 3-month follow-up period after implantation made it possible to evaluate the patency of the graft, both simply and noninvasively. It also permitted visualization of the connected abdominal aorta and renal and common iliac arteries having smaller caliber (diameter; less than 1 mm). In addition, the degree of the stenosis or aneurysm could also be detected. 3-Tesla MRA allowed the simplified and noninvasive assessment of the status on the vascular graft, including the formation of a stenosis or aneurysm, in the same rat at different times, which will be contributing to enhance the development of tissue-engineered vascular grafts even with small caliber. © 2009 Wiley Periodicals, Inc. J Biomed Mater Res Part B: Appl Biomater 92B: 156–160, 2010

Keywords: small-caliber vascular grafts; magnetic resonance angiography; animal implantation; biotube; tissue engineering

INTRODUCTION

Small-caliber arterial substitutes are needed for cardiac and peripheral revascularization procedures. For such small artery bypass grafting procedures, autologous arterial (e.g., internal thoracic artery and radial artery) or venous (e.g., saphenous vein) grafts still remain the most ideal vascular substitutes.[1,2] However, many patients do not have a vessel suitable for use owing to the poor quality, inadequate size or length, or previous harvest of such vessels. Moreover, a second surgical procedure is required to initially obtain the necessary vessel. Vascular prostheses, such as expanded polytetrafluoroethylene (ePTFE) and poly (ethylene terephthalate) (Dacron) grafts, have been used clinically for reconstructing arteries.[3] However, small-caliber (<6 mm) arterial substitutes have generally proved inadequate largely because of the formation of thromboses and intimal hyperplasia.[4,5]

Many design criteria have been proposed for the development of functional small-caliber arterial replacement grafts.[5–11] All most of all artificial vascular grafts (inner diameter, 1.5–3.0 mm) have been employed for transplantation

Correspondence to: Y. Nakayama (e-mail: nakayama@ri.ncvc.go.jp)

to rat abdominal aortas as an *in vivo* model.[6–8] Graft patency has been evaluated during the follow-up period by angiography[8] or by direct inspection at the time of removal for histological evaluation.[6,7] However, angiography requires cannulation of the carotid artery,[8] and a midline laparotomy is needed for direct inspection.[6,7] As a consequence, these methods are complex and invasive. Therefore, it is difficult to evaluate graft patency repeatedly in the same rat. Although, graft patency has also been evaluated by palpating the femoral pulse,[7] this method is subjective and uncertain.

The current imaging systems, including fluorescence antibody method, single photon emission computed tomography (SPECT),[12] laser doppler system,[13] or high-resolution ultrasound[14] for blood flow imaging in addition to magnetic resonance angiography (MRA), are powerful tool in tissue engineering field. However, it is considered that no imaging systems except for MRA fit for evaluation of the status of implanted small-caliber vascular grafts.

In clinical practice, MRI has been used as a noninvasive evaluation method for the assessment of brain blood vessels and peripheral arteries and also been widely used in preclinical research on experimental small rodents.[15–18] The studies have typically been aimed at understanding the patho-physiological status and evaluating the efficacy/side effects of newly developed treatments, such as pharmaceutical and regenerative medicine.

Our purpose in this study was to evaluate the status of a tissue-engineered vascular graft with inner diameter of 1.5 mm, clinically, repeatedly, and noninvasively in a rat implantation model. To this end, 3-Tesla contrast-free time-of-flight magnetic resonance angiography (TOF-MRA) was applied.

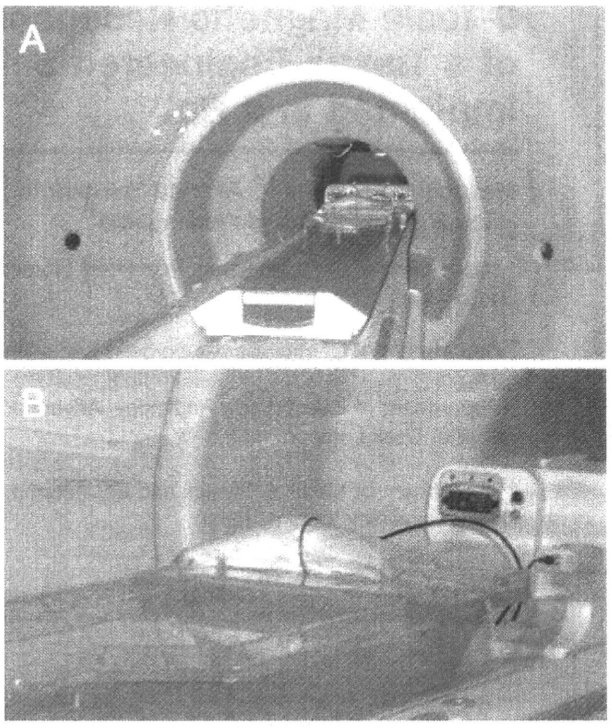

Figure 1. Experimental setup in MR imaging on a human whole-body 3T-MR scanner (GE Healthcare) (A). The coil was placed at the center of the gantry and its turn axis had perpendicular alignment to the static magnetic field (B). Rat's abdomen was positioned inside the coil along the craniocaudal direction. [Color figure can be viewed in the online issue, which is available at www.interscience.wiley.com.]

MATERIALS AND METHODS

Preparation and Implantation of the Connective Tubular Tissue

All animal experiments were conducted in accordance with local regulations, complying with the Principles of Laboratory Animal Care (formulated by the National Society for Medical Research) and the Guide for the Care and Use of Laboratory Animals (NIH Publication No. 86–23, revised 1985). The research protocol (No. 8050) was approved by the ethics committee of the National Cardiovascular Center Research Institute.

The connective tubular tissue was prepared by *in vivo* tissue engineering according to the previous reported method.[9] Briefly, a silicone rod (diameter, 1.5 mm; length, 10 mm; Tigers Polymer, Osaka, Japan) was used as a mold. One adult female Wistar rat (weight; 300 g) was anesthetized with 1.5% isoflurane (vol/vol air). The mold was placed in a dorsal subcutaneous pouch, and after 2 weeks, the implant was removed. The tubular tissue was obtained from the implant after trimming the peripheral tissues and pulling out the rod. The tube thus obtained was treated by coating with Argatroban (1 mg/graft; Mitsubishi Chemical Co., Tokyo, Japan) to make it antithrombogenic. It was then implanted to the infrarenal abdominal aorta of the same rat using an end-to-end anastomosis under microscopic guidance and sutured using 12 interrupted 10–0 nylon stitches [Figure 1(A)]. Patency was examined at the time of surgery by direct inspection. The wound was closed with 4–0 silk sutures. Thereafter, the rat had free access to standard food and water. Graft status was evaluated at 2, 36, and 78 days after transplantation by contrast-free TOF-MRA under anesthesia induced by an intramuscular injection of pentobarbital (40 mg/kg).

MR Data Acqusition

A human whole-body 3-Tesla magnetic resonance imaging (MRI) scanner (Signa, GE Healthcare, Milwaukee, WI) was employed in this study (Figure 1). The gradient coil system was capable of providing a maximum gradient amplitude of 40 mT/m. All sequence programs employed in this study were designed for clinical studies. A developed single-turn surface coil of 62 mm diameter was used for MR imaging [Figure 1(B)]. Contrast-free TOF-MRA was performed using a three-dimensional flow-compensated fast spoiled gradient recalled (3D-FSPGR) sequence [repetition

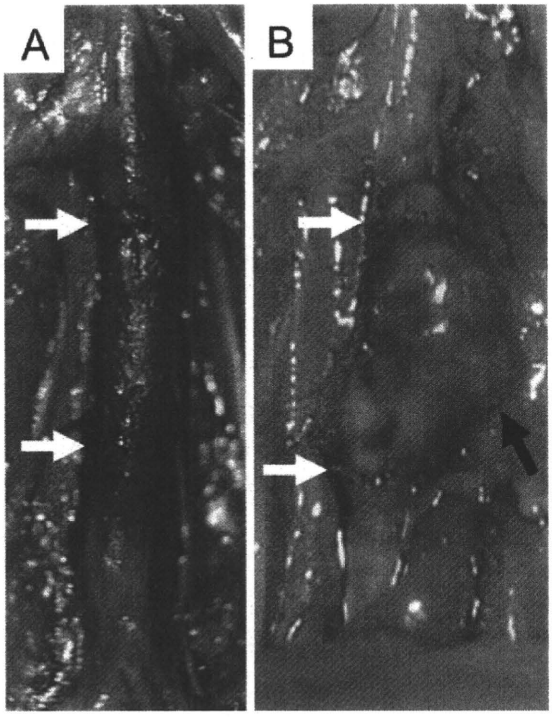

Figure 2. (A) The tubular connective tissue vascular graft (diameter; 1.5 mm) after autoimplantation in the rat infrarenal abdominal aorta (diameter; 1.3 mm) performed by end-to-end anastomosis under microscopic guidance using 12 interrupted stitches of 10-0 nylon suture. (B) The tubular connective tissue formed an aneurysm (max diameter; 3.0 mm) at 78 days after autoimplantation. White arrows indicate the proximal and distal anastomosis regions. Black arrow indicates the aneurysm. [Color figure can be viewed in the online issue, which is available at www.interscience.wiley.com.]

time (TR) = 21 ms, echo time (TE) = 5.4 ms (out of phase), flip angle (FA) = 15°, slice thickness = 0.4 mm, field of view (FOV) = 80 mm × 60 mm, matrix = 288 × 192, locs per slab = 128, the number of excitations (NEX) = 1, scanning time = 5 min 58 s]. For suppressing venous signals, a region of 40-mm thickness on the caudal side of the measured slab was saturated. The measured voxel size in TOF-MRA was 0.278 × 0.291 × 0.400 mm. The image reconstruction was zero-filled to a matrix size of 512 × 512 and the voxel size was 0.156 × 0.156 × 0.400 mm. MR angiograms were analyzed by generating the partial maximum intensity projection (pMIP) with a commercial software package (AZE, Tokyo, Japan). Our previous report on TOF-MRA was shown detail in rat.[13]

RESULTS

The tubular connective tissue with a diameter of 1.5 mm was autoimplanted successfully into the 1.3 mm diameter abdominal aorta of the rat by end-to-end anastomosis [Figure 2(A)]. After suturing with 12 interrupted stitches, there was little bleeding from either of the sites of anastomosis, indicated by the arrows in Figure 2(A). The patency of the graft was recognized directly by the satisfactory pulsation at the graft and distal side of the aorta.

3-Tesla contrast-free TOF-MRA of the rat was performed at 2 days after implantation [Figure 3(A)] to evaluate the status of the graft. The measurement time was ~6 min and no contrast medium was needed. The MRA distinctly visualized the patent graft connected to the abdominal aorta together with renal arteries and common iliac arteries of 0.7 and 0.8 mm diameter, respectively. Spatial resolution in the MRA was less than several hundred microns. A mechanical stenotic lesion, which may have been due to the anastomosis, was observed in both anastomosis regions. At 36 days after implantation, little stenosis and no aneurismal dilation of the graft were observed [Figure 3(B)]. At 78 days after implantation, the maximum diameter of the aneurysm formed at the graft was 3.0 mm [Figure 3(C)]. The shape of the aneurysm was very close to that observed macroscopically [Figure 2(B)]. Therefore, the status of the graft could be precisely determined, repeatedly, and noninvasively.

DISCUSSION

This study is the first to demonstrate the application of MRA to the evaluation of the status of a small-caliber arti-

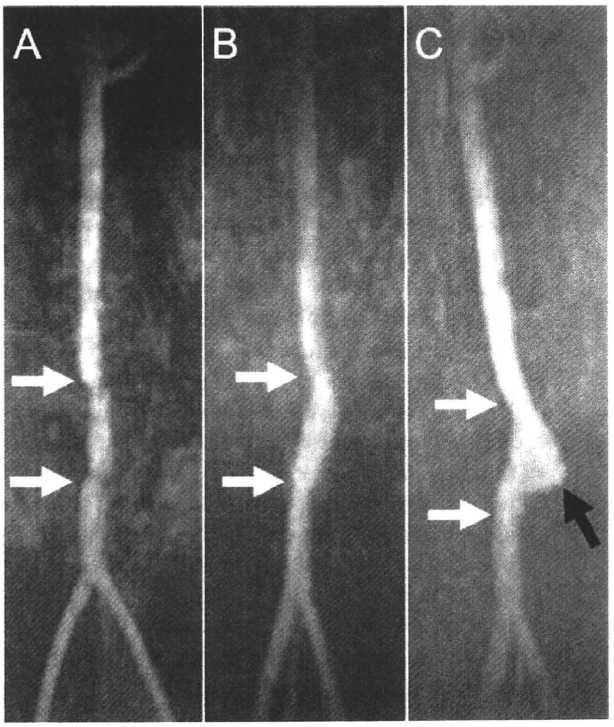

Figure 3. 3-Tesla contrast-free TOF-MRA images of the rat abdominal aorta at 2 (A), 36 (B), and 78 (C) days after autoimplantation of the biotube vascular graft. White arrows indicate the proximal and distal anastomosis regions of the abdominal aorta. A stenotic lesion was visible in the anastomosis regions at 2 days. An aneurysm formation in the graft was visible at 78 days (black arrow indicates the aneurysm).

ficial vascular graft implanted in the abdominal aorta of a rat. In the development of small-caliber vascular grafts as a preclinical study, *in vivo* evaluation is needed. Implantation studies have been performed mostly by using the abdominal aorta of rats.[6–8] Their certain patency must evaluate with sacrificing every observation periods, which is both labor-intensive and time-consuming when performing a large number of experiments. Since some rats survive with no symptoms after graft occlusion, assessment of the occlusion of an abdominal aorta after graft implantation is not possible solely on the basis of the rat's appearance. On the other hand, some researchers have evaluated graft patency by palpating the femoral pulse[7]; however, this method is prone to subjectivity and uncertainty. Therefore, evaluation of graft patency should be performed by direct inspection under laparotomy. On the other hand, even in histological observations, the evaluation of the degree of graft stenosis is very difficult.

In this study, MRI images of a reasonable quality were obtained from a rat using a human whole-body MRI scanner at 3-Tesla. Contrast-free TOF-MRA was able to depict the implanted graft with a diameter of ~1.5 mm, connected to the abdominal aorta with a diameter of ~1.3 mm, and also revealed arteries with diameters of less than 1 mm, such as the renal, common iliac, and tail arteries. In addition, an evaluation of the graft status, including the stenosis, was also feasible due to the high resolution and reasonable contrast. As indicated in Figure 3(A), the mechanical stenosis was clearly indicated at both sites of anastomosis. Furthermore, the aneurysm formation was clearly observed [Figure 3(C)]. Since the observation by MRA is simple and noninvasive, assessment of the status of small-caliber vascular grafts could be performed in the same rat at different times. The repeatable MRA observation in a single rat enabled correct assessment of the graft status over the follow-up period. Such repeatability will reduce the variation in results stemming from individual difference in experimental animals.

As a model graft for implantation in this study, the tubular connective tissue was used. The tissue was prepared similar to biotubes.[9] Biotubes are autologous prosthetic tubular tissues prepared by in-body tissue architecture technology. The biotube, obtained from rats by embedding the silicone rods (diameter; 3 mm) into their subcutaneous pouches for 4 weeks, had several 10 μm in thickness, about 500 gf in maximum load at rapture, and about 1000 mmHg in burst pressure.[19] This technology, a novel and practical concept in regenerative medicine, is based on the phenomenon of tissue encapsulation of foreign materials *in vivo*, and it can be used to develop autologous tissues of the desired shape, depending on the mold design.[9–11] Using this technology, several types of tissues, including "biotubes" as vascular tissues,[9–11] "biovalves" as tri-leaflet heart valve-shaped tissues,[20,21] and "biocovered stents" as hybrid IVR devices,[22] have been developed. In this study, by shortening of the encupsulation period weak and ununiform wall structure was prepared particularly for observation of the variety of vascular graft fate. As expected, normal, stenosis, or aneurysm models were appropriately obtained in one rat.

The assessment of graft status using MR imaging does, however, have limitations. When using certain materials for artificial grafts (e.g., ePTFE and Dacron), MR imaging might be difficult owing to graft artifacts. Furthermore, such as ultrasound and/or digital subtraction angiography, it is difficult to evaluate blood stream by 3D evaluation. The TOF-MRA is more appropriate for the evaluation of tissue-engineered vascular grafts. The signal-to-noise ratio in image quality on TOF-MRA is strongly dependent on the static field strength and the coil design. Further study should be needed in developing coil. We hope that others who study at understanding the patho-physiological status and evaluating the efficacy/side effects of newly developed treatments, such as pharmaceutical and regenerative medicine.

CONCLUSIONS

Contrast-free TOF-MRA with 3-Tesla allowed an assessment of tissue-engineered small-caliber vascular graft status in the rat systemic arterial circulation. As the protocol used in this study is simple and noninvasive, it is useful for the longitudinal evaluation of graft status in the rat; this will contribute to enhancing the development of tissue-engineered small-caliber vascular grafts, particularly in the field of regenerative medicine.

REFERENCES

1. Tomizawa Y. Vascular prostheses for aortocoronary bypass grafting: A review. Artif Organs 1995;19:39–45.
2. Ferrari ER, Von Segesser LK. Arterial grafting for myocardial revascularization: How better is it? Curr Opin Cardiol 2006; 21:584–588.
3. Zilla P, Bezuidenhout D, Human P. Prosthetic vascular grafts: Wrong models, wrong questions and no healing. Biomaterials 2007;28:5007–5027.
4. Pasquinelli G, Freyrie A, Preda P, Curti T, D'addato M, Laschi R. Healing of posthetic arterial grafts. Scanning Microsc 1990;4:351–362.
5. Isenberg BC, Williams C, Tranquillo RT. Small-diameter artificial arteries engineered in vitro. Circ Res 2006;98:25–35.
6. Doi K, Nakayama Y, Oka T, Matsuda T. A new microporous polyurethane vascular graft prepared by an excimer laser ablation technique. ASAIO J 1995;41:M608–M611.
7. Campbell JH, Efendy JE, Campbell GR. Novel vascular graft grown within recipient's own peritoneal cavity. Circ Res 1999; 85:1173–1178.
8. Pektok E, Nottelet B, Tille JC, Gurny R, Kalangos A, Moeller M, Walpoth BH. Degradation and healing characteristics of small-diameter poly (epsilon-caprolactone) vascular grafts in the rat systemic arterial circulation. Circulation 2008;118:2563–2570.
9. Nakayama Y, Ishibashi-Ueda H, Takamizawa K. In vivo tissue-engineered small-caliber arterial graft prosthesis consisting of autologous tissue (Biotube). Cell Transplant 2004;13: 439–449.

10. Sakai O, Kanda K, Ishibashi-Ueda H, Takamizawa K, Ametani A, Yaku H, Nakayama Y. Development of the wing-attached rod for acceleration of "Biotube" vascular grafts fabrication in vivo. J Biomed Mater Res B Appl Biomater 2007; 83:240–247.
11. Watanabe T, Kanda K, Ishibashi-Ueda H, Yaku H, Nakayama Y. Development of biotube vascular grafts incorporating cuffs for easy implantation. J Artif Organs 2007;10:10–15.
12. Kempen DH, Yaszemski MJ, Heijink A, Hefferan TE, Creemers LB, Britson J, Maran A, Classic KL, Dhert WJ, Lu L. Non-invasive monitoring of BMP-2 retention and bone formation in composites for bone tissue engineering using SPECT/CT and scintillation probes. J Control Release 2009; 134:169–176.
13. Hobo K, Shimizu T, Sekine H, Shin'oka T, Okano T, Kurosawa H. Therapeutic angiogenesis using tissue engineered human smooth muscle cell sheets. Arterioscler Thromb Vasc Biol 2008;28:637–643.
14. Mccarthy I. The physiology of bone blood flow: A review. J Bone Joint Surg Am 2006;88:4–9.
15. Brockmann MA, Kemmling A, Groden C. Current issues and perspectives in small rodent magnetic resonance imaging using clinical MRI scanners. Methods 2007;43:79–87.
16. Yamamoto A, Sato H, Enmi J, Ishida K, Ose T, Kimura A, Fujiwara H, Watabe H, Hayashi T, Iida H. Use of a clinical MRI scanner for preclinical research on rats. Radiol Phys Technol 2009;2:13–21.
17. Smith DA, Clarke LP, Fiedler JA, Murtagh FR, Bonaroti EA, Sengstock GJ, Arendash GW. Use of a clinical MR scanner for imaging the rat. Brain Res Bull 1993;31:115–120.
18. Guzman R, Lövblad KO, Meyer M, Spenger C, Schroth G, Widmer HR. Imaging the rat brain on a 1.5 T clinical MR-scanner. J Neurosci Methods 2000;97:77–85.
19. Huang H, Zhou YM, Ishibashi-Ueda H, Takamizawa K, Ando J, Kanda K, Yaku H, Nakayama Y. *In vitro maturation* of "Biotube" vascular grafts induced by a 2-day pulsatile flow loading. J Biomed Mater Res B Appl Biomater 2009 [Epub ahead of print].
20. Hayashida K, Kanda K, Yaku H, Ando J, Nakayama Y. Development of an in vivo tissue-engineered, autologous heart valve (the biovalve): Preparation of a prototype model. J Thorac Cardiovasc Surg 2007;134:152–159.
21. Hayashida K, Kanda K, Oie T, Okamoto Y, Sakai O, Watanabe T, Ishibashi-Ueda H, Onoyama M, Tajikawa T, Ohba K, Yaku H, Nakayama Y. "In vivo tissue-engineered" valved conduit with designed molds and laser processed scaffold. J Cardiovasc Nurs 2008;23:61–64.
22. Nakayama Y, Zhou YM, Ishibashi-Ueda H. Development of in vivo tissue-engineered autologous tissue-covered stents (biocovered stents). J Artif Organs 2007;10:171–176.

Multicenter Evaluation of a Standardized Protocol for Rest and Acetazolamide Cerebral Blood Flow Assessment Using a Quantitative SPECT Reconstruction Program and Split-Dose ^{123}I-Iodoamphetamine

Hidehiro Iida[1,2], Jyoji Nakagawara[1,3], Kohei Hayashida[1,4], Kazuhito Fukushima[1,5], Hiroshi Watabe[1,2], Kazuhiro Koshino[1,2], Tsutomu Zeniya[1,2], and Stefan Eberl[1,6]

[1]Dual-Table Autoradiography SPECT Research Group in Japan, Osaka, Japan; [2]National Cerebral and Cardiovascular Center–Research Institute, Osaka, Japan; [3]Nakamura Memorial Hospital, Sapporo, Japan; [4]Takeda Hospital, Kyoto, Japan; [5]National Cerebral and Cardiovascular Center–Hospital, Osaka, Japan; and [6]Royal Prince Alfred Hospital, Sydney, Australia

SPECT can provide valuable diagnostic and treatment response information in large-scale multicenter clinical trials. However, SPECT has been limited in providing consistent quantitative functional parametric values across the centers, largely because of a lack of standardized procedures to correct for attenuation and scatter. Recently, a novel software package has been developed to reconstruct quantitative SPECT images and assess cerebral blood flow (CBF) at rest and after acetazolamide challenge from a single SPECT session. This study was aimed at validating this technique at different institutions with a variety of SPECT devices and imaging protocols. **Methods:** Twelve participating institutions obtained a series of SPECT scans on physical phantoms and clinical patients. The phantom experiments included the assessment of septal penetration for each collimator used and of the accuracy of the reconstructed images. Clinical studies were divided into 3 protocols, including intrainstitutional reproducibility, a comparison with PET, and rest–rest study consistency. The results from 46 successful studies were analyzed. **Results:** Activity concentration estimation (Bq/mL) in the reconstructed SPECT images of a uniform cylindric phantom showed an interinstitution variation of ±5.1%, with a systematic underestimation of concentration by 12.5%. CBF values were reproducible both at rest and after acetazolamide on the basis of repeated studies in the same patient (mean ± SD difference, −0.4 ± 5.2 mL/min/100 g, n = 44). CBF values were also consistent with those determined using PET (−6.1 ± 5.1 mL/min/100 g, n = 6). **Conclusion:** This study demonstrates that SPECT can quantitatively provide physiologic functional images of rest and acetazolamide challenge CBF, using a quantitative reconstruction software package.

Key Words: ^{123}I-iodoamphetamine; cerebral blood flow; acetazolamide; SPECT; vascular reactivity; quantitation

J Nucl Med 2010; 51:1624–1631
DOI: 10.2967/jnumed.110.078352

Received Apr. 27, 2010; revision accepted Jul. 14, 2010.
For correspondence or reprints contact: Hidehiro Iida, Department of Investigative Radiology, National Cerebral and Cardiovascular Center–Research Institute, 5-7-1 Suita City, Osaka 565-8565, Japan.
E-mail: iida@ri.ncvc.go.jp

Current clinical practice using SPECT relies largely on interpretation of qualitative images reflecting physiologic function. Quantitative functional parametric images may be obtained by applying mathematic modeling to SPECT data corrected for attenuation and scatter. Quantitative regional cerebral blood flow (CBF) (*1–3*) and cerebral vascular reactivity (CVR) in response to acetazolamide challenge (*4–6*) have been obtained with these techniques. One major application of such quantitative SPECT (QSPECT) approaches is the evaluation of ischemic status in patients with occlusion or stenosis in their middle cerebral arteries, to provide prognostic information of the outcome of revascularization therapies (*7*). Quantitative analysis in SPECT has also been demonstrated in the assessment of binding potential for several neuroreceptor ligands (*8,9*), for the quantitative assessment of regional myocardial perfusion (*10,11*), and for the assessment of radioaerosol deposition and clearance in healthy and diseased lungs (*12*). However, providing the standardized quantitative approach required for multicenter clinical trials has so far received only limited attention. Challenges remain in providing consistent quantitative data across institutions using a variety of SPECT equipment and vendor-specific reconstruction strategies (*13*). This limitation is attributed to a lack of standardized procedures in the reconstruction software offered by vendors, particularly in terms of correcting attenuation and scatter. Kinetic modeling for physiologic parameter estimation is also not part of the vendors' standard SPECT software. Although separate packages can be purchased for this purpose, they are not integrated and are flexible general-purpose packages, requiring considerable skill and knowledge to effectively use. Thus, they are not ideal for routine clinical use.

Scatter and attenuation occur in the object and are thus object-dependent but are not dependent on the geometry of the imaging equipment (*14*). Therefore, once a software program is developed to provide accurate image reconstruction with compensation for both attenuation and scatter, the